UNIVERSITY OF SOUTHERN QUEENSLAND

Starspots on the Active Young Solar-Type Star AH Lep

A dissertation submitted by
Keith John Treschman
BSc, MEd, BA

For the Award of
Master of Science

Department of Biological and Physical Sciences
University of Southern Queensland

October 2010

Abstract

Young solar-type stars inform us about the early evolution of objects that form a major component of the stellar population of our galaxy.

Single active young solar-type stars close to the Sun's mass also provide us with proxies for the Sun's early history, its activity and underlying magnetic dynamo.

The active young solar-type star AH Lep provides a convenient target to image its magnetic activity in detail.

AH Lep is of particular interest because of its relatively modest rotation rate ($v \sin i$ = 28 km s^{-1}) compared with other previously studied active stars; in other words, this star represents the opportunity to study the effects of rotation on the dynamo of young solar-type stars.

This thesis investigates the starspot features and magnetic field of AH Lep using the techniques of Doppler and Zeeman Doppler Imaging, resulting in a tomographic map of the star and magnetic field detections.

In contrast to the large polar spot features of more rapidly rotating active solar-type stars, mid-latitude starspots predominate on AH Lep. At the time of observation at least, AH Lep displayed little in the way of a polar spot and instead showed large spot features more reminiscent of the Sun today than the polar spot dominated appearance of rapid and ultrarapid rotators. Total spot coverage (3.3%) is not small but is significantly less than that of rapid rotators.

The magnetic field of AH Lep was detected in a number of observations and a tentative magnetic map was constructed. More observations under the most favourable conditions are needed to investigate more fully the magnetic topology of the star.

Certification of Dissertation

I certify that this dissertation contains no material accepted for the award of any other degree or diploma in any university. To the best of my knowledge, it contains no material published or written by another person, except where due reference is made in the text.

_____ _____

Signature of Candidate Date

ENDORSEMENT

_____ _____

Signature of Supervisor Date

Acknowledgements

Four years ago when I decided I was interested in pursuing further studies in Astronomy I commenced the process of seeing what was on offer externally at the universities around Australia. I had enrolled but not started at another institution before I had a meeting with Brad Carter at the University of Southern Queensland (USQ) in Toowoomba where I was residing at that time. I was instantly impressed with his passion for his subject so that I changed my course immediately.

Brad became my supervisor for the duration of this Masters. He has provided the inspiration and suggestion for this thesis, taught me some of the intricacies of the computing and procedures necessary for this work, put me in contact with personnel associated with this line of investigation and accompanied me to the Anglo-Australian Telescope (AAT) to gather data. His guidance has been the correct match of allowing me to proceed with my own learning but knowing when to step in to save much wasted time when I hit a roadblock or travelled too far into a side channel.

I have appreciated our conversations about Astronomy and other topics. He has also given me the encouragement and sensible advice at the times later in the course when my resolve was wavering.

The original data which I was permitted to use were gathered at the AAT by Meir Semel (Observatoire de Paris Meudon), Jean-François Donati (Laboratoire d'Astro-physique, Observatoire Midi-Pryénées Toulouse France), John Barnes (University of St Andrews Scotland), Stephen Marsden (then at USQ) and Brad Carter (USQ). I extend my gratitude to these collaborators.

Stephen Marsden now at the AAT has been very helpful with sharing his expertise on the procedures to process the data and providing information on his more recent research. Ian Waite (Toowoomba Grammar School) has assisted me also with procedural elements and his latest results.

The AAT has provided me with the opportunity to resource data and be on-site for my own research. The personnel there provide a wonderful and extensive service.

My wife Madonna has witnessed my study over many years. I appreciate her ability to put things in perspective and provide the touch of encouragement when I need it mostly.

Finally, I wish to acknowledge my own students. While I attempt to model lifelong learning to them I also receive the impetus from them to continue as I witness their dedication and commitment to their own study pursuits.

Contents

List of Figures

List of Tables

Chapter 1 Introduction

As our closest star the Sun has an enormous influence on the Earth. However, the present is but a brief moment in the history of the Sun and Earth. Knowledge of the powerful winds and radiation from the young Sun assists in our understanding of the early history and atmospheres of the rocky planets (Guinan et al. 2009). On Earth the protection afforded by its magnetosphere should also have helped in the development of life forms within 4 x 10^8 years of its formation (Freedman and Kaufmann 2005). The importance of stellar magnetic fields on the variability of young stars is well known and is relevant to the conditions on any attendant planets (Lister et al. 2009) and the study of the habitability of extrasolar planets.

The Sun is the only star whose surface has been imaged directly in any detail. As such it can act as a model for stars of a similar type. In turn, the study of like stars of different ages allows the possibility of inferring the evolution of the Sun and its future path. Of specific interest are very young stars. Since planetary accretion from the solar nebula was probably completed in less than 100 x 10^6 years (Wetherill 1980), stars in this age group may stand as a proxy for the Sun at the time of Earth's formation (Dorren and Guinan 1994).

Whereas the Sun is G2V, AH Lep is a G3V star (Wichmann et al. 2003) with an age no more than 50 x 10^6 years (Wichmann and Schmitt 2003), making it a useful representative of the young Sun. AH Lep is variable and classified as a BY Draconis star. These are cool emission-line dwarfs showing quasiperiodic light changes with periods from a fraction of a day to 120 days and amplitudes from several hundredths to 0.5 magnitude in the visual spectrum. The light variability is caused by the axial rotation of a star with a variable degree of nonuniformity of the surface brightness (spots) and chromospheric activity (Samus, Durlevich et al. 2004). These cool dwarfs have active chromospheres and are considered important for the investigation of magnetic activity produced by stellar dynamos. They link to an understanding of the magnetic activity of the Sun (Carroll and Ostlie 2007) with AH Lep a proxy for the Sun's early activity.

1.1 The Sun

The Sun is a G2 star on the main sequence with a mass of 1.989 x 10^{30} kg, radius of 6.955 x 10^{8} m and age 4.57 x 10^{9} years (Carroll and Ostlie 2007). As a nearby and well studied object, the Sun provides the basis for our understanding of many other stars.

1.1.1 Solar Magnetic Activity

The activity of the Sun is understood in terms of its magnetic field which energises and controls a range of solar phenomena, from sunspots and prominences to flares and coronal mass ejections. The most obvious and familiar example of solar activity is the presence of sunspots and the sunspot cycle.

1.1.1.1 Sunspots

In 1609 Galileo Galilei commenced his telescopic observations of sunspots and noted that they varied in number and position. Counts since 1700 have revealed that the number rises to a maximum and decreases to a minimum over an average of 22 years. This cycle is also evident when the average daily sunspot area as a percentage of the visible hemisphere is plotted against the date. The cycle begins with sunspots occurring at around $\pm 40^{\circ}$ latitude. They remain at constant latitude and have a lifetime of around a month. Succeeding sunspots form at lower latitudes and the cycle shows a movement towards the equator where they terminate. The maximum number occurs at intermediate latitudes and the minimum when the first sunspots appear. (Figure 1.1)

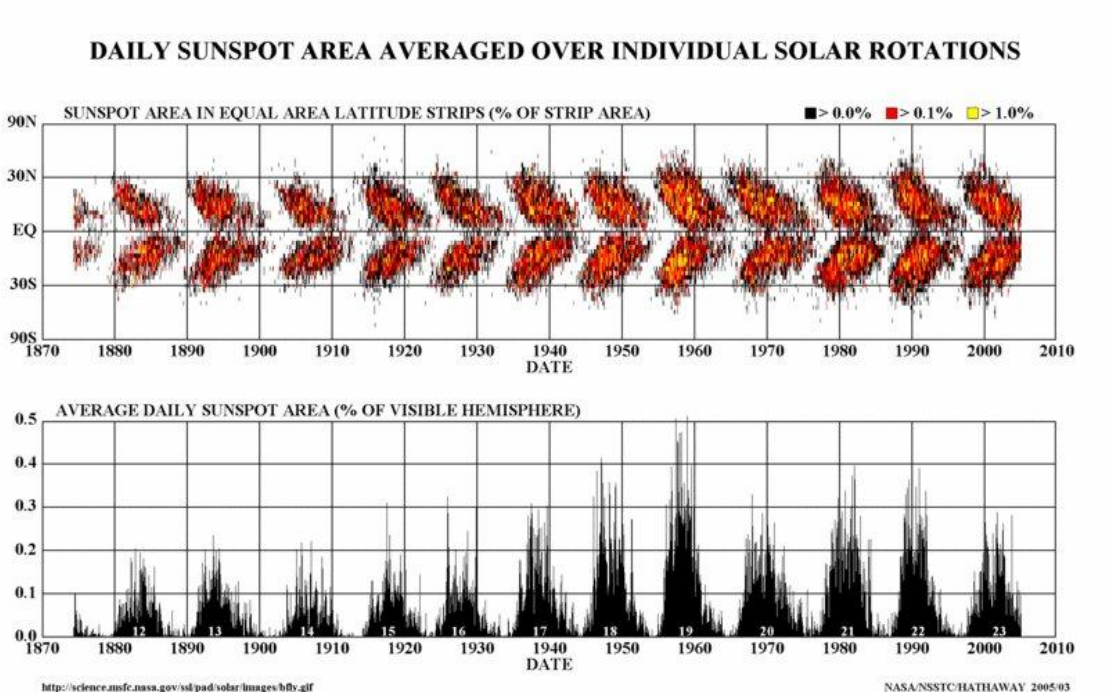

Figure 1.1 The upper diagram shows the migration of the sunspots towards the equator in each cycle and the lower one the changes to the amount of coverage of the solar surface over time during the period 1874-2004. Diagram from D.H. Hathaway, NASA http://upload.wikimedia.org/wikipedia/commons/9/93/Sunspot_butterfly_with_graph.jpg

The structure of a sunspot entails an umbra which can have a diameter of 30 000 km surrounded by a penumbra. Magnetism within a sunspot is detected by observation of its spectral lines. The Zeeman Effect gives a measure of the strength and polarity of the magnetic fields. The amount of splitting of the lines is proportional to the strength of the magnetic field and the polarisation of the light indicates its direction. Sunspots come in pairs where the leading one in the direction of rotation of the Sun has the same polarity as the hemisphere it is in and the trailing one the opposite polarity. The magnetic field in the umbra is vertical and it becomes horizontal across the penumbra. At a sunspot minimum there is a reversal of the Sun's dipolar field so the pattern repeats in a 22 year cycle.

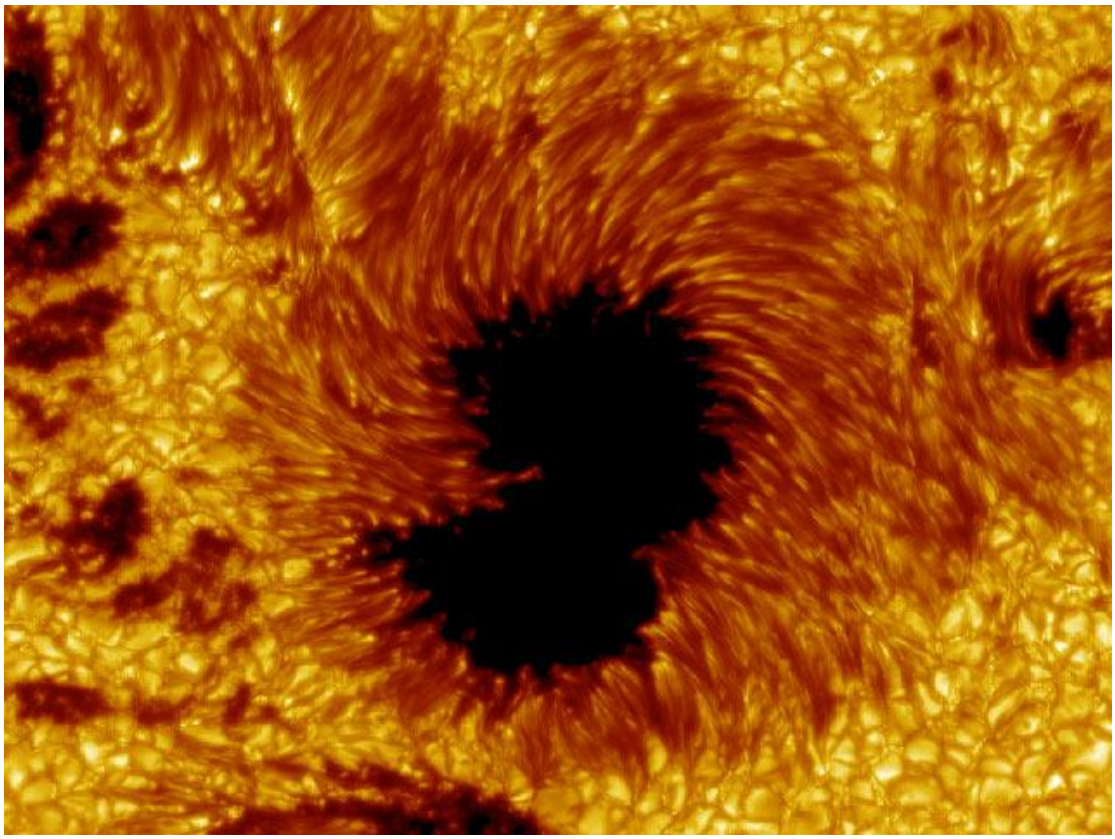

Figure 1.2 Sunspot shows the darkening compared with the surrounding surface. http://media.skyandtelescope.com/images/Sunspot-group_l.jpg Image is from the Swedish one metre Solar Telescope and is courtesy of the Swedish Academy of Sciences.

The dark appearance of a sunspot is due to its temperature of typically 3 900 K being cooler than the surrounding photosphere (T_{eff} = 5 777 K) and hence producing reduced thermal emission in the optical spectrum (Figure 1.2). Sunspots indicate the interference with subsurface photospheric convection where strong magnetic fields emerge from the solar interior.

1.1.2 The Solar Interior

A model for the Sun's interior (Figure 1.3) consists of a core to 0.3 of its radius. As a result of a temperature at the centre of 1.570 x 10^7 K, a pressure of 2.342 x 10^{16} N m^{-2} and a density of 1.527 x 10^5 kg m^{-3} (Bahcall et al. 2001), conditions permit nuclear reactions to take place via the proton-proton chain where the effective reaction is

$$4\ {}^{1}_{1}\mathrm{H} \rightarrow {}^{4}_{2}\mathrm{He} + 2 \text{ positrons} + 2 \text{ electron neutrinos} + 2 \text{ photons}.$$

In the lifetime of the Sun the mass fraction of its centre has altered from 0.71 to 0.34 for H and 0.27 to 0.64 for He.

As the pressure, temperature and density of the interior of the Sun decreases from the centre, a point is reached at 0.3 of the radius where nuclear reactions cease. From here to 0.714 of the radius a new zone occurs where radiation dominates energy transport. Here, energy is continually absorbed and emitted on its journey to the exterior.

The outer zone represents a layer where the temperature has fallen to 2×10^6 K at the base and so some of the heavier metals are not completely ionised. This increases the opacity of the interior so convection becomes a more efficient means of energy transport than radiation.

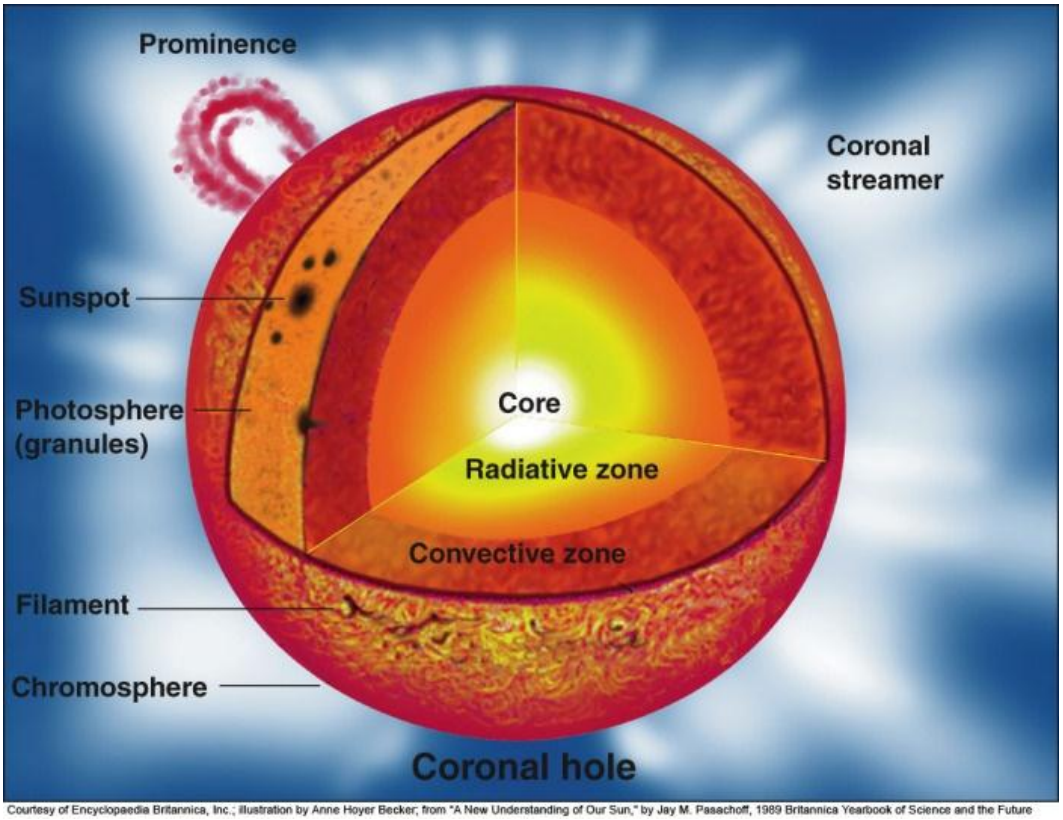

Figure 1.3 Solar Interior shows the core, radiative zone and convective zone.
From http://www.ifa.hawaii.edu/~barnes/ast110_06/tsaas/1003a.jpg

A Michelson Doppler Imager (MDI) on board the SOHO spacecraft allows a plot of rotation rate versus latitude for the Sun and can take measurements within the Sun

(Figure 1.4). Pressure waves resulting from turbulence in the convection zone have certain frequencies amplified by constructive interference. Changes in the propagation of these oscillation waves are detected with images over time or by the Doppler shift of the photospheric absorption lines. From this the inner structure of the Sun is inferred. Consequently, it is seen that there is a differential rate of rotation in the convective zone but the radiation zone behaves like a solid body.

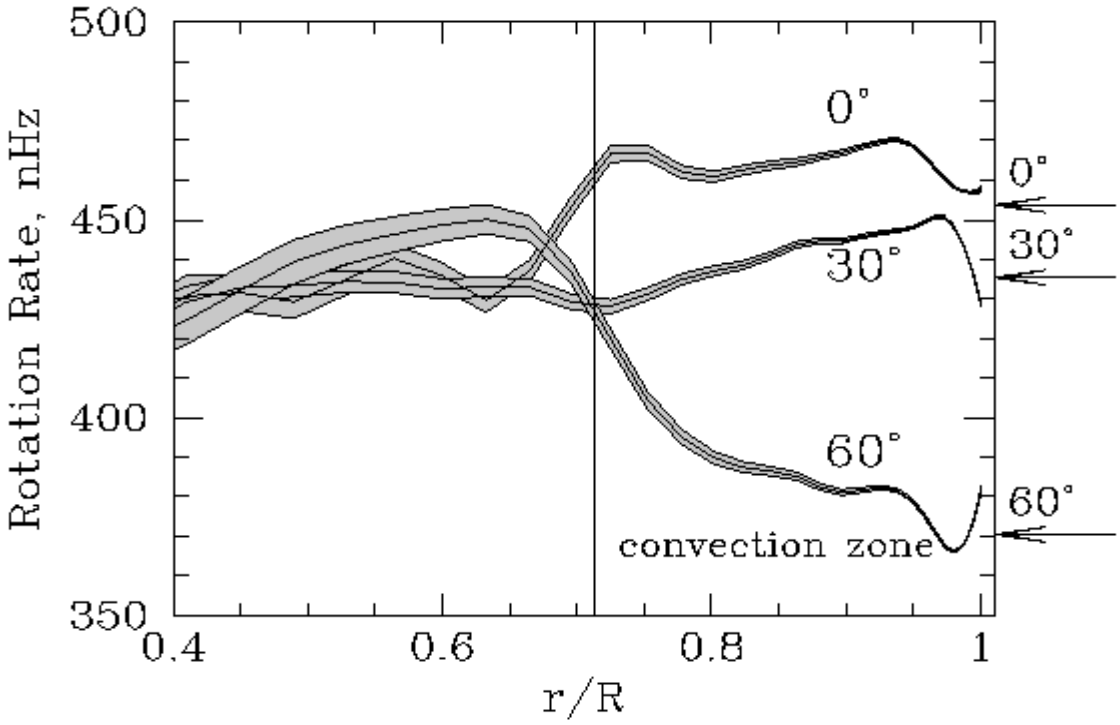

Figure 1.4 Image courtesy of SOHO (ESA and NASA). The horizontal axis label r/R is the fraction of the depth from the surface of the Sun to its radius. Measurements with MDI show differential rotation rate for latitude in the convective zone but there is a clear demarcation once the radiative zone is reached.
From http://sohowww.nascom.nasa.gov/gallery/Helioseismology/mdi013.html.

1.2 The Solar Dynamo

The boundary between the radiative and convective zones is a discontinuity where fluid flow is vastly different on either side. The consequence is a shearing effect caused by

rotation which results in electric currents in the highly conducting plasma, in turn giving rise to the solar magnetic field.

1.2.1 The Babcock Model

In 1961 Babcock outlined a mechanism to explain the features of the magnetic cycle of the Sun in three stages (Figure 1.5).

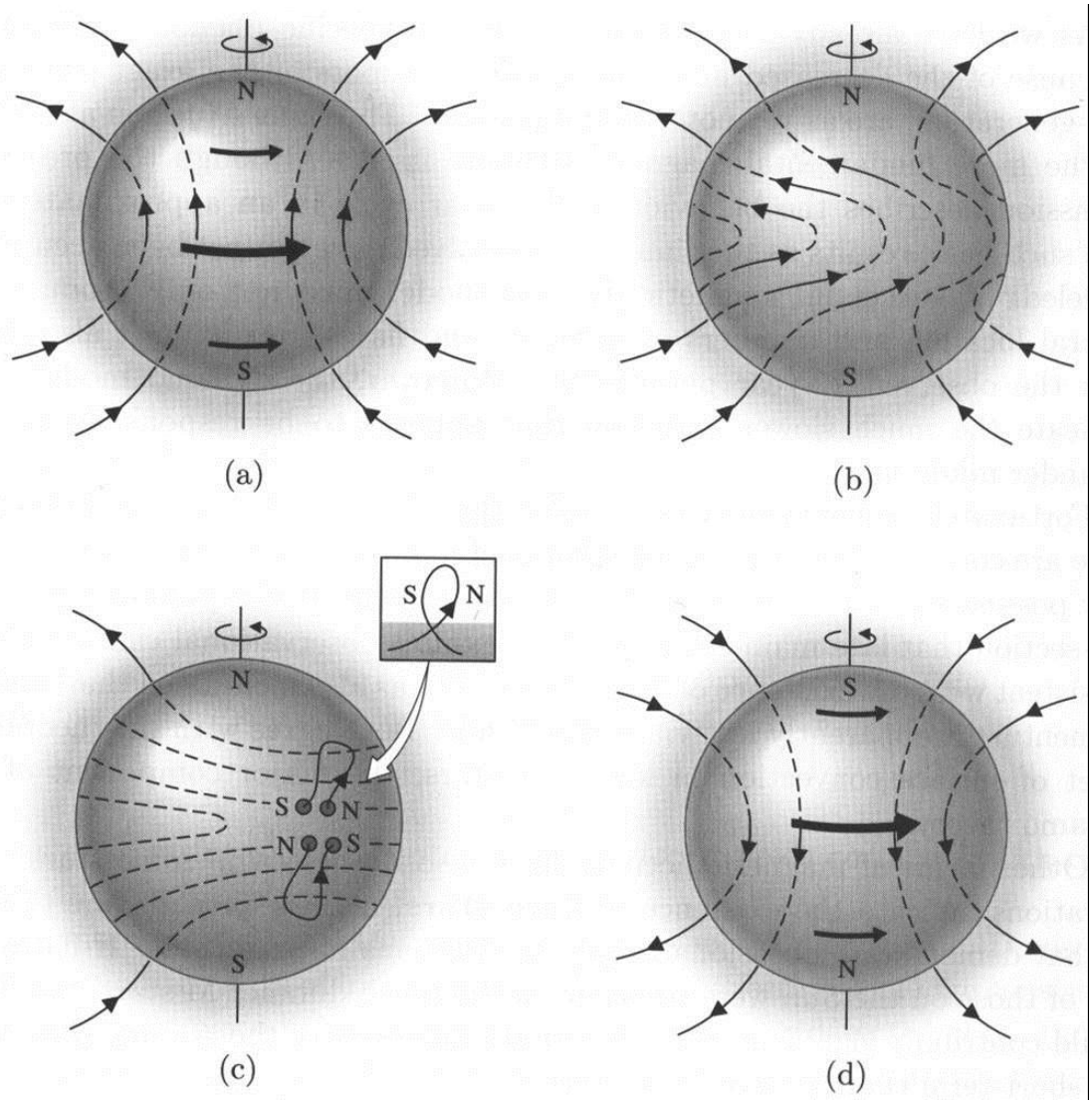

Figure 1.5 The Babcock model of the solar magnetic cycle shows (a) the initial field (b) twisted by rotational differences into (c) magnetic ropes which recombine at the equator to (d) reverse the field. From *An Introduction to Modern Astrophysics* (2nd edition) by B W Carroll and D A Ostlie (Pearson Education).

1.2.1.1 Stage 1: The Ω Effect

The magnetic field lines within the plasma are initially poloidal (towards the poles). Differential rotation of the Sun drags these lines along and overlays this structure with a component which is toroidal (same direction as lines of latitude). This wrapping of the field lines around the Sun is called the Ω effect.

1.2.1.2 Stage 2: Surface Eruption and the α Effect

The α effect is the creation of magnetic ropes that are regions of intense magnetic fields caused by the turbulence in convective cells. The magnetic pressure resulting from the stronger field creates buoyancy where the ropes rise to the surface and are visible as sunspots. Because of the magnetic field along the rope, this explanation answers the question of why each lead spot has the same polarity in one hemisphere but the opposite in the other.

1.2.1.3 Stage 3: Opposite Polarity

The twisting commences at higher latitudes during a minimum in the solar cycle. With more turbulence the ropes are twisted into knots so that sunspots appear at lower latitudes as the cycle moves to a maximum. Cancellation of the polarities occurs at the poles until such time that the poloidal field is reconnected but with opposite polarity.

1.2.2 A Refined Model

The Babcock model has been successful in explaining the broad details of the solar cycle. However, it is unable to predict the timing of the cycle, features of the Maunder minimum, decreased flux flow at sunspots or the generation of flares.

Refinements are provided by Schrijver and Zwaan (2000). Neighbouring active regions may produce more complex fields than the simple dipolar one. The convective zone has regions of different densities resulting in a variation in the flow of energy along different directions. The outward flow of matter may be weaker than the inflow and not as constrained. The inflow turbulence and differential rotation may be amplified by the α effect. The process may be repeated so the field is far from organised as in the

Babcock model. It is the stronger fields that survive and emerge at the surface as a bipolar field.

Close to the poles the trailing polarity reconnects with the poloidal field so that the leading polarity connects somewhere else. The equatorial regions connect across hemispheres to produce the opposite polarity.

1.3 Solar-Type Stars

Many features of the solar dynamo have been modelled but there is still a raft of details to be understood. These include the process by which there is a decreased flux from sunspots, the mechanism of flare generation, the timescales that exist and the state of the dynamo for the Maunder minimum (Carroll and Ostlie 2007). Hence, a study of other stars allows comparisons and contrasts which can lead to a better understanding of the dynamo process.

The Sun is a main sequence G2 star with a radiative and convective zone outside its core. Near the surface of a star a decreasing mass is connected with a decreasing temperature so that opacity increases because of the presence of hydrogen ionisation. Thus, convection becomes more efficient than radiation for a stellar mass less than 1.3 solar masses. For still lower masses the base of the convective zone extends further into the star, until for stars of 0.3 solar masses, the mechanism of energy transfer outside the core is totally convective (Carroll and Ostlie 2007). Thus, the range of 1.3 to 0.3 solar masses is here classed to include solar-type stars as larger mass is associated with a lack of a convective zone and a lower mass operates in a totally convective fashion. These restrictions include stars from mid-F to early-M spectral types.

1.3.1 Stellar Dynamos

Solar-type stars could be theorised to have dynamo processes like the Sun. Observations support this concept as well as similar atmospheric magnetic phenomena such as flares and starspots (Carroll and Ostlie 2007).

In the Sun the regeneration of the poloidal field is due to the α effect which gives a periodicity and asymmetry in the field structure but for other cool stars theory

proposes it could be caused by either the α or Ω effect, depending on the stars. The Ω term is stronger in the conversion of the poloidal field into a toroidal one. However, the latter conversion could be due more to the α effect which gives a symmetrical arrangement as in the Earth, or equal contributions from the α and Ω effects to the generation of the toroidal field.

The current thinking proposed by Barnes (2003) from an analysis of the rotation period for solar and late-type stars places them on two sequences. The rapid rotators only have a convective distributed dynamo (*C* sequence). There is no coupling between the convective and radiative zones so there is inefficiency in the depletion of angular momentum. The outer zone is spun down on an exponential timescale and no large-scale dynamo exists. As age increases there is a smaller fraction of stars in this category. A connection or reconnection is established between these zones so that the shear between them sets up the large-scale magnetic field associated with the dynamo. These are given the appellation I sequence (interface). Exterior winds now drive off some of the angular momentum so they decrease their rotation rates. The drive from *C* to I occurs across a *gap*. The time spent on this *gap* is longer for lower stellar masses. Thus, this theory makes a connection between rotation rate and the mass and age of a star. Further, young G stars are proposed to evolve to the I sequence in 10^8 years. The conclusion is that the interface between the radiative and convective zones eventually generates the solar dynamo.

A different model where the dynamo is distributed throughout the convective region of a star has been proposed by Donati et al. (1992; 1999; 2003a), Donati and Collier Cameron (1997) and Donati (1999) to explain the extended regions of an azimuthal (toroidal) magnetic field observed on some stars.

Granzer et al. (2000) theorise how it is possible that some stellar dynamos operate differently from the solar one. They propose that rapid rotators influence rising magnetic flux tubes so that they emerge at high stellar latitudes where the faster the rotation the greater the emergence latitude; there is a moderate decrease in the latitude with increasing stellar mass and a strong decrease in the emerging position with

increasing stellar age. These flux loops originate at the bottom of the convective zone and move upwards to near the surface. The Coriolis force is dominant in rapid rotators (Schüssler and Solanki 1992) which shifts the flux tube parallel to the axis of rotation due to the conservation of angular momentum. The actual latitude depends on the relative size of the radiative core. The buoyancy force which acts radially outwards depends on the magnetic field strength and the stratification of the convective zone (Schüssler et al. 1996). Magnetic tension and drag forces also need to be taken into account. The relative strengths of these forces are responsible for the spread of latitudinal emergence without resorting to a distributed dynamo explanation.

The existence of distributed dynamos may seem to give rise to some reservation with using solar-type stars to understand the Sun. However, since the Sun has dramatically slowed its rotation over time, the distributed dynamo model for rapidly rotating stars is useful in analysing the Sun's behaviour when a young and rapidly rotating star is on or near the zero age main sequence.

1.4 Stellar Magnetic Activity

Atmospheric magnetic phenomena on solar-type stars can be compared to the activity on the Sun. Since the internal structures are considered similar, it is assumed that their photospheric activity would be similar.

1.4.1 Starspots

Just as magnetic effects on the Sun cause cooling regions and hence sunspots, then starspots arise in a similar way. They are considered active regions under magnetic influence (Schüssler et al. 1994). Starspots are not able to be detected directly but may be inferred by three different techniques: photometry, Doppler Imaging and Zeeman Doppler Imaging.

1.4.1.1 Photometry

Stellar rotation causes a variation in brightness as the starspots move into view. Measurements may show a dip in brightness of typically about 0.1 magnitude or less.

Pulsation of a star will also produce changes in brightness and the presence of spots will only be favoured if the variation is at regular intervals which correspond to the rotation rate of the star. This technique can locate the starspot in longitude but not as readily in latitude.

1.4.1.2 Doppler Imaging

A spectroscopic method called Doppler Imaging also produces the starspot distribution. It requires a stellar rotation of $v \sin i$ roughly between 20-250 km s^{-1} and an inclination angle of 20-70°. For low rotation rate resolution is not possible whereas for faster rates the lines may be too shallow to discern spots. If $i = 0°$, the line of sight is along the pole and no Doppler Effect exists. For $i = 90°$, the sight along the equator will give a mirror image symmetry so that no distinction can be made between the hemispheres.

In a similar way to photometry the presence of cooler regions on the surface of a star causes a small reduction in the intensity of the continuum contribution across the spectral line profile. However, a lower amount of light is absorbed at the Doppler shift of the starspot relative to the centre of the line. The result is a small bump in an absorption spectrum.

Since the star is rotating, this bump will appear firstly on the blue-shifted, short wavelength side as the starspot approaches the observer. It will move across the line profile. On recession from the observer, the starspot and corresponding spectral line bump moves to the red-shifted, longer wavelength side. This Doppler Effect broadening of the spectral lines is illustrated in Figure 1.6. The movement of the starspot across the stellar disc due to its rotation results in a change in the Doppler shift dependent on latitude. Equatorial starspots are visible for half the stellar rotation cycle so they trace a sinusoidal curve of velocity with an amplitude equal to $v \sin i$. Higher latitude starspots produce sinusoidal curves with lower amplitudes in a regressive fashion. The proportional visibility of a starspot in a rotation cycle depends on its latitude and the inclination of the stellar rotation axis to the line of sight. Longitudes are detected by the times at which starspot signatures cross the centre of the line profile. Latitudes are related to the sinusoidal amplitudes. (Collier Cameron 2000)

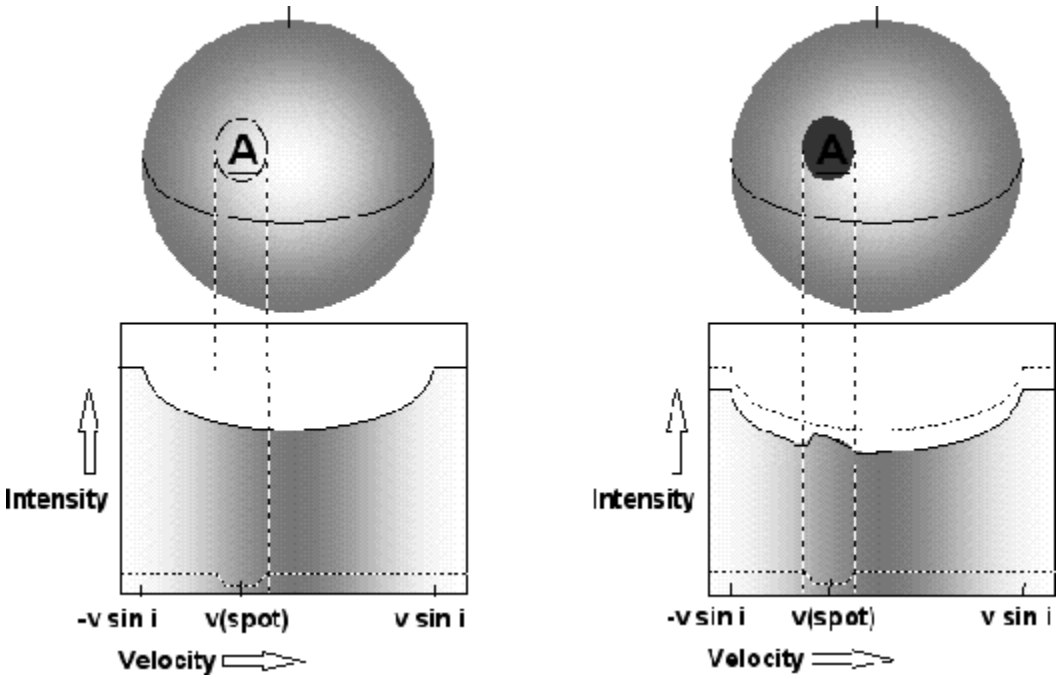

Figure 1.6 The Doppler Effect of a rapidly rotating star is shown as a broadening of a spectral line in the left image and a bump and reduced intensity due to the spot in the right image. From http://star-www.st-and.ac.uk/~acc4/coolpages/cartoon.gif. Image courtesy Andrew Collier Cameron, University of St Andrews.

The Sun currently has a *v* sin *i* value of 2.0 km s^{-1}, so stars with the rapid rotation producing observable Doppler Imaging signatures in their spectra are young, rapidly rotating stars or those in evolved close binaries where rapid rotation can be maintained. Apart from EK Dra measured by Strassmeier and Rice (1998) as 17.3 ± 0.4 km s^{-1}, *v* sin *i* values for the more than 50 stars targeted for Doppler Imaging are > 20 km s^{-1}. Marsden et al. (2004) measured VXR45A as high as 248 km s^{-1}.

The technique is based on a process of maximum entropy image reconstruction. A map was firstly produced by Vogt and Penrod (1983) and the method is described more fully in Vogt et al. (1987), Rice et al. (1989) and Hussain (1999).

Doppler Imaging has concentrated on F, G and K stars (Strassmeier 2001) and when polar spots exist the surface coverage is up to 10% (Donati et al. 2003a). As the method involves a minimisation to match the profiles, the actual surface coverage may

be much higher. This can be contrasted with the < 1% figure for the Sun and spots predominantly within a band ± 30° of the equator.

Those stars with deep convective zones are theorised to have polar spots (Schüssler et al. 1996 and Granzer et al. 2000). Polar spots should not be observed on zero-age main sequence stars. Instead, with an increasing rotational rate, the spots should appear at higher latitudes. The only way polar spots could be explained with this population is if the magnetic flux tubes migrate towards the pole.

Since polar spots and large surface coverage compared with the Sun do occur, it is proposed that the dynamo processes in these stars are both stronger than and qualitatively different from that in the present-day Sun.

1.4.1.3 Zeeman Doppler Imaging

The difficulty experienced with other techniques of imaging stellar surfaces is that areas of opposite magnetic polarity cancel each other. Zeeman Doppler Imaging (ZDI) can use Doppler Imaging and extend this with polarisation analysis to show the orientation of magnetic fields as proposed by Semel (1989).

The Zeeman Effect is the splitting of spectral lines in the presence of a magnetic field. The separation of the components is proportional to the magnetic field strength. It arises from the polarisation of radiation which is a non-random distribution of the electric vectors of the photons in a beam (Kitchin 2003).

The polarisation of starlight was interpreted firstly in an attempt to understand some of the properties of interstellar magnetic fields. In ZDI, two types of polarisation are described: linear (when the electric vectors are all parallel and their direction is constant) and circular (when the angle of the electric vector rotates with time at the frequency of the radiation). They are different aspects of partially elliptically polarised radiation as displayed in Figure 1.7.

The properties of the partially elliptically polarised light are described by four Stokes parameters I, Q, U, V (Kitchin 2003). Respectively, they fix the total intensity of the optical beam, the preponderance of linearly horizontal polarised light over linearly vertical polarised light, the linear + 45° polarisation over linear - 45° component and the

preponderance of right circularly polarised light over the left circularly polarised contribution.

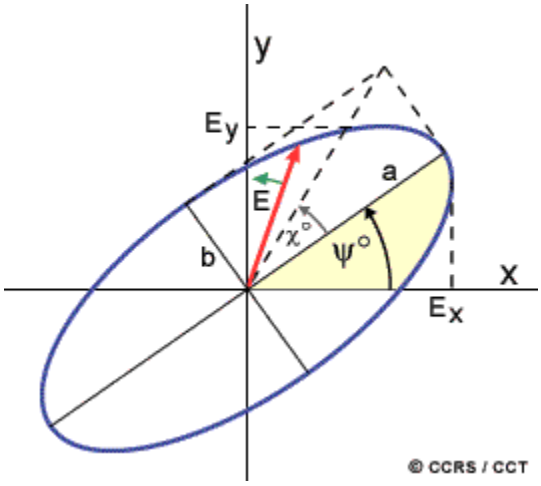

Figure 1.7 A polarisation ellipse shows the electric vector *E* tracing this particular shape. From http://cct.rncan.gc.ca/glossary/index_e.php?id=3173

The technique of ZDI has been elaborated by Semel (1989), Donati et al. (1989), Brown et al. (1991), Donati and Brown (1997) and Donati et al. (2003a). A brief description follows.

Regions of equal projected velocity on a star have their spectral lines broadened in a similar way due to the Doppler Effect. Any surface magnetic activity will influence the polarisation of light from that region. Observations can be effected in left- and right-circularly polarised light. With measurements of I, $I + V$ and $I - V$ obtained, subtraction between $I + V$ and $I - V$ can lead to V. This signature provides the information on the location and polarity of any magnetic regions by the use of iterative reconstructions of the magnetic field vectors. All magnetically sensitive lines in the spectrum behave in the same way (Carter et al. 1996). The technique is displayed in Figure 1.8.

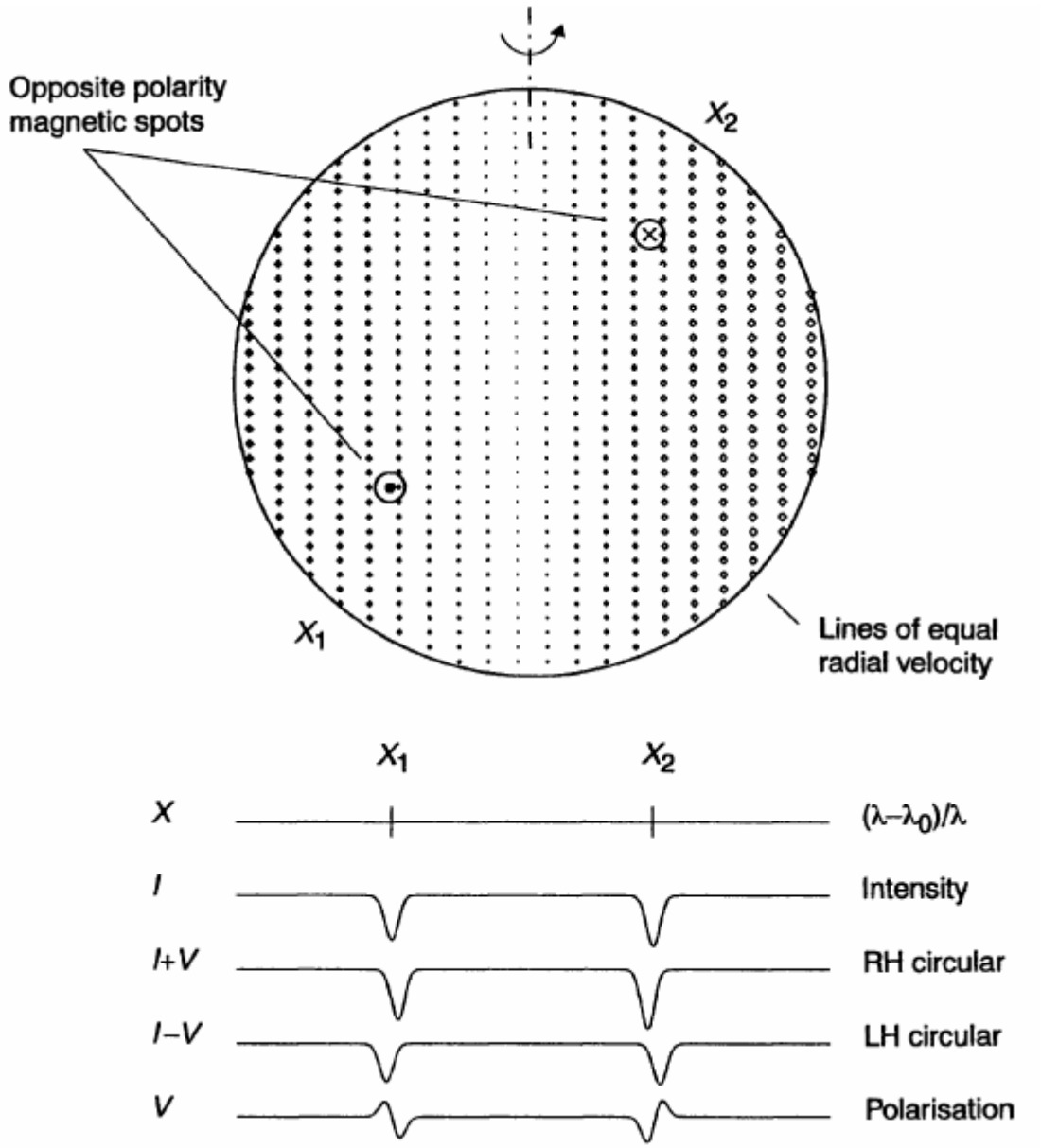

Figure 1.8 Principles of Zeeman Doppler Imaging. Two arbitrary magnetic regions of opposite polarity are present on the stellar disc. The contributions to the stellar spectral line from each of the spots appear at X_1 and X_2, separated by a Doppler shift in the wavelength domain. The intensity spectrum is I. Each magnetic field induces small opposite wavelengths shifts of the corresponding absorption profile in the right- and left hand circularly polarised spectra ($I + V$ and $I - V$ respectively).The difference between the profiles $I + V$ and $I - V$ leads to V and this has a characteristic shape based on the location of the magnetic regions on the surface of the star. Image from Carter et al, 1996.

Limitations on obtaining a magnetic signature involve the brightness of a star and instrumental polarisation. As the signatures are very small at 0.1% of the continuum

level, special techniques are used to enhance the signal extraction of the captured light. These are explained in chapter 2.

Donati et al. (2003a) have developed software to map stellar magnetic fields into their radial, azimuthal (toroidal) and meridional (poloidal) components.

The results to hand show the azimuthal element to be the most significant (Donati et al. 2003a) and this is why a number of researchers have postulated that unlike the modern-day Sun where an interface between layers is probably responsible for the dynamo, these stars may embody a distributed dynamo (Donati et al. 1992, 1999, 2003a, Donati and Collier Cameron 1997, Donati 1999).

1.4.2 Differential Rotation

The outer layer of the Sun does not rotate like a solid body. The variation in rotation period is from 25 days at the equator to 35 days near the poles.

For other stars both Doppler Imaging and ZDI lend themselves to measures of differential rotation by tracking either starspots or magnetic activity over time.

This can also be achieved spectroscopically by reconstructing a single image from images taken at different times and using a simplified differential rotation law that has been applied to the Sun (Petit et al. 2002). Another method adopted by Weber et al. (2005) cross-correlates images over time also with a solar rotation law. Thirdly, Collier Cameron et al. (2002) follow particular spots on the stellar surface.

All stars studied by these techniques display differential rotation. Donati et al. (2003b) have shown that different rates are obtained from different methods. This is related to the different depths upon which each method is operating and is a way of inferring the interior structure of some stars.

Donati et al. (2003b) and Collier Cameron and Donati (2002) have found significant differences in rates between stars and for the one star at different times, for example, for the two stars AB Dor and LQ Hya. In order to obtain magnetic intensities they assume that the changes in kinetic energy from the altering rotation rates are transferred to the magnetic energy throughout the entire convective zone. They caution, however, that the magnetic field would be expected to be intermittent within

this zone and that potential energy changes due to the changing shape of the star would need to be included.

1.5 The Active Young Solar-Type Star AH Lep

AH Lep is an active young solar-type star whose physical parameters (as displayed in Table 1.1) suggest that it is a suitable new target for Zeeman Doppler Imaging.

1.5.1 Stellar Data for AH Lep

Table 1.1 Physical properties of AH Lep from various sources with the Sun as a comparison.

Property	AH Lep	Reference	Sun [k]
Spectral Type	G2V, G3V,G, F5	a, b-d, e, f-g	G2V
Bolometric Magnitude	8.46 – 8.50	b	-26.76
Magnitude (Standard V Photometric Band)	4.94	calculated page 20	4.83
U-B	0.13	b	0.195
B-V	0.64	b and h	0.65
V-R	0.37	b	
V-I	0.70	b	
Log X-ray Luminosity (W)	22.6	d	2-6
Effective Temperature (K)	5 680	calculated page 20	5 770
Age (x 10^6 y)	< 50	e	4 600
Right Ascension (epoch 2000)	05h 34' 09".163	i	
Declination (epoch 2000)	-15º 17' 03".18	i	
Proper Motion in RA (mas y^{-1})	25.6	i	
Proper Motion in Dec (mas y^{-1})	-22.3	i	
Galactic Longitude (epoch 2000)	218°.521	i	
Galactic Latitude (epoch 2000)	-23°.844	i	
Parallax (mas)	28.6 ± 7.10	c	
Distance (pc)	28-46, 48	b, a	

v sin *i* (km s^{-1})	30, 28	d and j, b and h	2.0
Radial Velocity (km s^{-1})	24.1 ± 2.0, 24.9 ± 2-3	c, d	
Rotation Period (d)	1.31 ± 0.01	j	25.4
Width of Li I line (mÅ)	260, 230	h, d	
Width of Li I line corrected for Fe I (mÅ)	224	d	
Delta Li I line (mÅ)	35	d	
Galactic Velocity *U* (km s^{-1})	-14.86 ± 1.56, -6.2	c, d	10.0
Galactic Velocity *V* (km s^{-1})	-18.31 ± 1.62, -12.3	c, d	5.25
Galactic Velocity *W* (km s^{-1})	-7.52 ± 1.00, -1.1	c, d	7.17

a. Burleigh et al. 1998; b. Cutispoto et al. 1999 ; c. Montes et al. 2001 ; d. Wichmann et al. 2003; e. Wichmann and Schmitt 2003; f. Smithsonian Astrophysical Observatory 1966; g. Positions and Proper Motions Catalogue 1993 ; h. Messina et al. 2001 ;
i. Tycho Catalogue 1996, 2000; j. Cutispoto et al. 2003b ; k. Dorren and Guinan 1994
The galactic velocity measurements use the right-handed coordinate system where *U* is towards the galactic centre, *V* is in the direction of the galactic rotation and *W* is towards the north galactic pole.

The F5 classification comes from a 1966 catalogue of the Smithsonian Astrophysical Observatory (SAO 150571) and a 1993 improvement in astrometric data in the Positions and Proper Motions Catalogue (PPM 215961). However, Burleigh et al. (1998), in their search data from the International Ultraviolet Explorer 1978-1996, ROSAT 1990-1999 (2RE JO534-151 and 2RE JO53410-151648) and the Extreme Ultraviolet Explorer 1992-2000 where count rates and luminosities were used, found this star to be G2V (HD 36869). G3V arises from more recent observations in 1995 of high-precision UBV$(RI)_c$ photometry by Cutispoto et al. (1999) at the European Southern Observatory in Chile as well as the Wide Field Camera on ROSAT.

Cutispoto et al. (1999) comment that the optical variability of 0.04 magnitudes that was detected for the first time on this star is likely to be the result of photospheric spots. Messina et al. (2001) give the amplitude change as 0.09 magnitudes.

The Tycho Catalogue used an auxiliary star mapper on the Hipparcos Space Astrometry Mission. The spacecraft was designed to measure the position, parallax and

proper motion of a large number of stars. Published in 1996 this catalogue had less precision than the Hipparcos Catalogue also printed in 1996. In 2000 the Tycho-2 Catalogue was produced (TYC 5916-792-1).

A wide range in stellar distance is given for AH Lep. For a G3V star, if the luminosity L is taken as 0.9 that of the Sun, then from

$$M = M_{Sun} - 2.5 \log_{10} \frac{L}{L_{Sun}} \text{ and } M_{Sun} = 4.83 \quad (1)$$

the absolute magnitude of AH Lep emerges as 4.94. If this value and the brightness magnitude of 8.46 are placed in

$$m - M = 5 \log_{10} d \text{ in pc} - 5 \quad (2)$$

the distance value is 50 pc, slightly higher than the literature values in Table 1.1 of 28-46 and 48 pc. Some difference is, however, expected given that AH Lep is a young star for which a main sequence luminosity has to be treated with caution. Nevertheless, from the Stefan-Boltzmann equation

$$L = 4\pi R^2 \sigma T_e^4 \quad (3)$$

for a radius R = 0.98 that of the Sun, the Stefan-Boltzmann constant σ, the effective absolute temperature T_e of the star and the effective surface temperature of the Sun taken as (5 777 K) the following equation

$$\frac{L}{L_{Sun}} = \left(\frac{R}{R_{Sun}}\right)^2 \left(\frac{T_e}{T_{e\,Sun}}\right)^4 . \quad (4)$$

produces an effective surface temperature of AH Lep of 5 680 K.

Further to the discussion in section 1.3.1, Barnes (2003) derives a measurement of age from the rotation rate and colour dependence for the *I* and *C* sequences. In the *I* case

$$P = t^{0.5} f(B - V) \quad (5)$$

where P is the rotation period in days, t is the age in Myr and the

$$\text{function of } (B - V) = (B - V - 0.5)^{0.5} - 0.15(B - V - 0.5). \quad (6)$$

P for AH Lep is 1.31 days and B – V is 0.64 giving an age of 14 x 10^6 years. For the *C* case

$$\ln\left(\frac{P}{0.2}\right) = \frac{t}{100}\left(B - V + 0.1 - \left(\frac{1.0}{3000}\right)t\right)^3 \quad (7)$$

and t = 44 x 10^6 years. Guinan and Engle (2003) studied solar-type stars and obtained the relationship for G stars

$$\log_{10}\left(\frac{1}{P}\right) = 1.865 - 2.854\ t^{0.08254} \quad (8)$$

for t in Gyr. This yields 2.6 x 10^6 years with a large uncertainty.

The zero-age main sequence (ZAMS) is where stars firstly reach the diagonal line in the Hertzsprung-Russell diagram and commence equilibrium hydrogen fusion. Bernasconi and Maeder (1996) displayed pre-main sequence evolutionary tracks and showed that the time for collapse onto the ZAMS is inversely related to mass. If AH Lep is taken as having the same mass as that of the Sun, this would equate to 38.9 x 10^6 years (Carroll and Ostlie 2007).

Another sign of extreme youth is a large lithium abundance (Zuckerman et al. 2001) which exists on AH Lep. Li is not an end product in the significant nuclear reaction chains and is destroyed by collisions with protons at temperatures greater than 2.7 x 10^6 K which occurs deep within the convective zone (Carroll and Ostlie 2007).

All the foregoing discussion of age places AH Lep as a very young star with a maximum age of 50 x 10^6 years. It has either just reached the ZAMS or is close to it.

1.6 Summary and Hypothesis

A description of the processes that power the Sun is gleaned, in the main, by observation of surface phenomena and these are influenced by magnetic fields. Thus, an understanding of the mechanism of the solar dynamo is crucial to gain an insight into our star.

Research has shown that solar-type stars exhibit features which are related to their magnetic dynamos. A study of starspots on AH Lep with the use of ZDI is important as it adds another candidate to the list of young solar-type stars which are rapid rotators and have characteristics indicative of strong magnetic dynamo activity.

Since the strength of a stellar magnetic field is assumed to depend on both spectral type and rotation rate (Collier Cameron and Jianke 1994), it is important to collect information on a wide variety of stars. As each piece of information is added to

the jig-saw puzzle, the aim is that the Sun can direct an understanding of the dynamo in similar stars and, in return, these stars may elucidate the picture inside the Sun, particularly, in its earlier years when the Earth was forming. Cutispoto et al. (2003a) indicate that young stars have high $v \sin i$, high Li abundance and high chromospheric/ coronal activity but these three properties should decrease with age. With sufficient candidates of a spread of ages, an indication of the evolutionary history of the Sun and its activity will emerge.

AH Lep has particular scientific value as a single young solar proxy for dynamo studies. Its mass is sufficiently close to that of the Sun to be a proxy indicator of the convective zones in the young Sun and sun-like stars. AH Lep's rapid but not extreme rotation also fits within the admittedly large range of rotation rates the young Sun could have conceivably displayed and offers a comparison with more extreme rotators to gauge the effect of rotation rate. Thus, AH Lep is a useful solar-like target intermediate in its dynamo activity between the Sun with its small low and mid-latitude spots and those very rapidly rotating stars with giant polar spots. This leads to a working hypothesis that Zeeman Doppler Imaging of AH Lep should display starspot and magnetic features that represent a transition between these two extremes. This thesis will therefore analyse data from Zeeman Doppler Imaging of AH Lep in an effort to understand its appearance and dynamo compared to and different from the Sun today and what is known about the spots, surface fields and dynamos of very rapidly rotating young solar-type stars.

Chapter 2 Instrumental Setup, Observations and Analysis

2.1 ZDI at the Anglo-Australian Telescope (AAT)

Telescope

Data were collected on the 3.893 m telescope of the Anglo-Australian Observatory (Figure 2.1) situated on Siding Spring Mountain (31˚ 17′ S, 149˚ 40′ E, 1 149 m above sea level) near Coonabarabran in New South Wales, Australia by Semel, Donati, Barnes and Marsden on 08, 09, 10 December 2003, these four observers plus Carter on 11 December 2003 and Marsden, Waite, Guggenberger, Carter, Treschman and Burton on 10 December 2008.

Semel Polarimeter

This is a visitor instrument developed at Observatoire de Paris-Meudon. It consists of Fresnel rhomb retarders which analyse polarised light over the entire spectral domain. It was mounted at the Cassegrain focus f/8 where light is collected through a 220 μm circular pinhole at the centre of the mirror on top of the polarimeter.

The device consists of a quarter-wave plate (axis at 45° to the axis of the beam) followed by a half-wave plate. Two polarisation states of left- and right-hand circular polarisation are transmitted along two fibres. A sequence consists of four separate exposures to measure the polarisation: P1-P2-P2-P1 for circularly polarised light (Stokes *V*). Rotation of the half-wave plate allows P2 to be 90° to P1. As the polarisation is alternated in each output fibre there can be an absence of spurious signals of polarisation from both the telescope and the polarimeter.

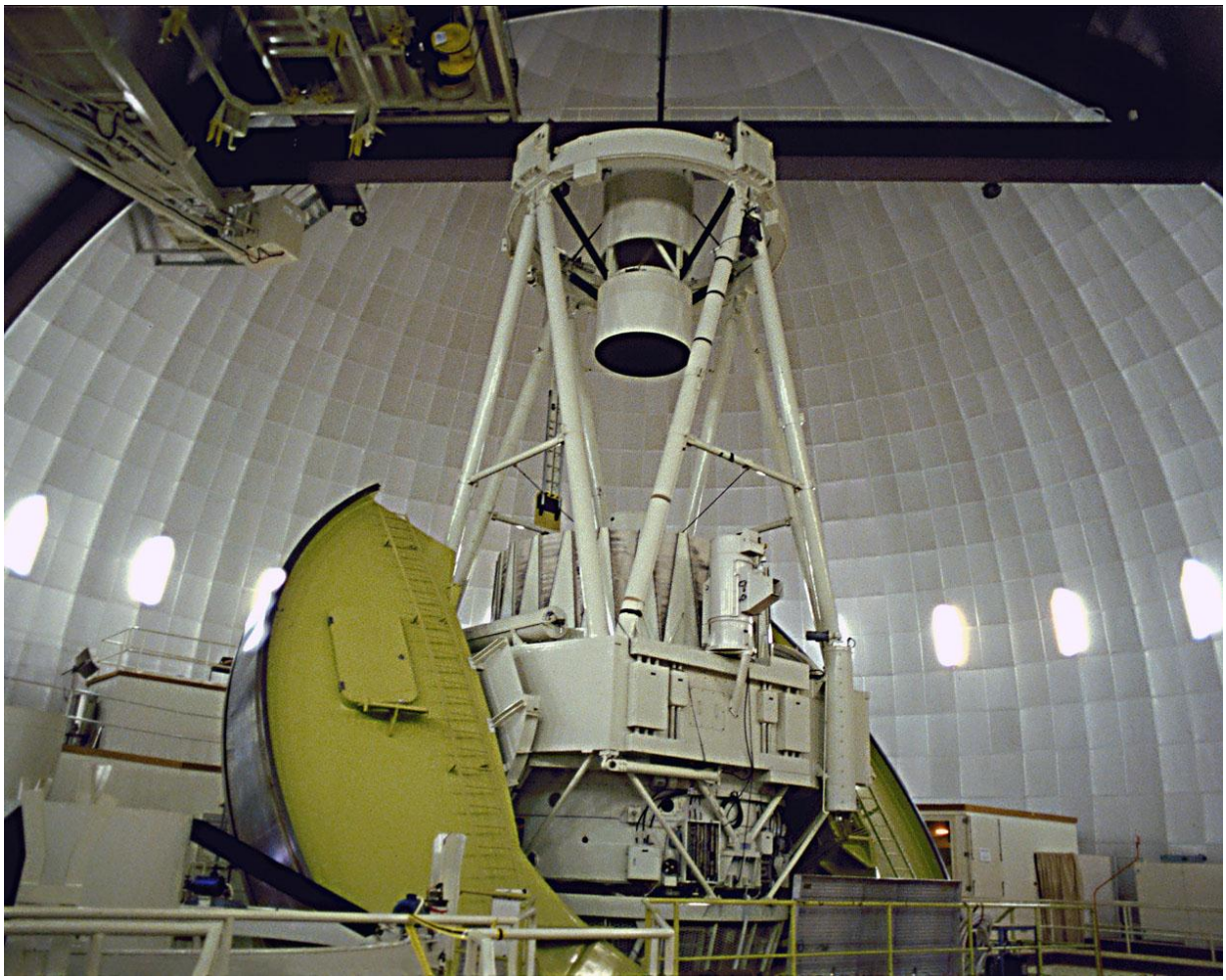

Figure 2.1 Anglo-Australian Telescope. Courtesy Michael A Stecker.
From mstecker.com/pages/australiaphotos1_fp.htm

Echelle Spectrograph

The University College London Echelle Spectrograph (UCLES) receives light from the telescope via a fibre feed and operates at the f/36 coudé focus (Figure 2.2).

An echelle grating (from the French échelle ladder, literally ladder rung, from Latin scāla, scale) (Macquarie 2002) is used for diffraction in spectroscopy when high resolution is required. It consists of a series of plates of equal thickness arranged in stepwise formation with a constant offset.

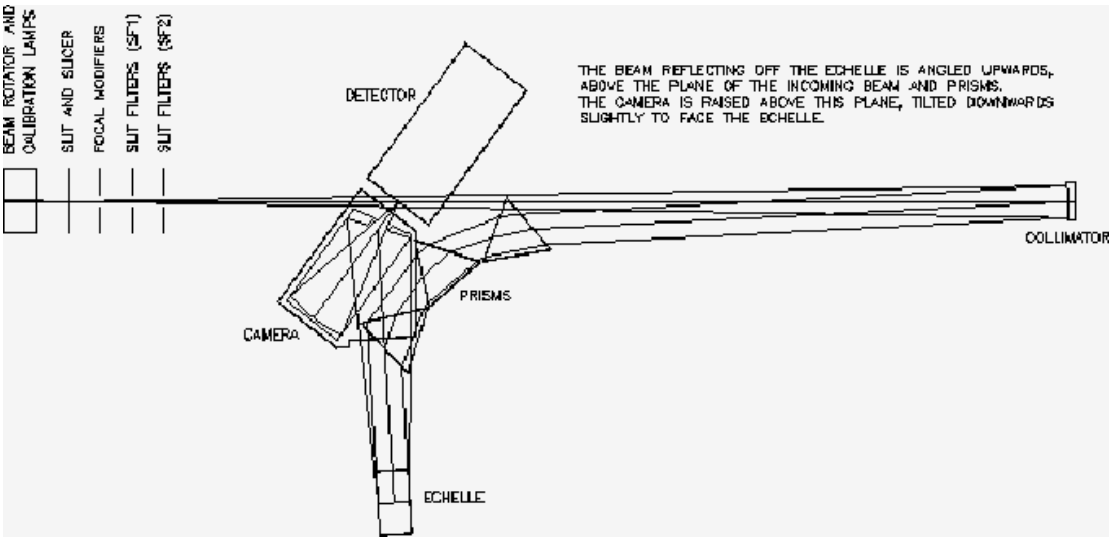

Figure 2.2 Echelle Spectrograph.
From http://www.astro.ljmu.ac.uk/courses/phys362/notes/img94.png

The UCLES offers high resolution, that is, $\frac{\lambda}{\Delta\lambda}$ = 5–8 x 10^4 combined with good wavelength coverage. The blaze angle, defined as that between the beam of light and the surface of the grating, is approximately 63˚ and it produces order numbers 50-150. The dispersion (µm mm^{-1}) is proportional to the wavelength and the dispersion at a given wavelength depends on the blaze angle and does not depend on the groove spacing. This device has two grating sizes, 31.6 and 79 lines mm^{-1}. The 31 grating gives almost continuous wavelength coverage at bluer wavelengths with short slit lengths of 6-15 arcsecond.

Light Path

The UCLES light path consists of calibration lamps ⇒ slit assembly ⇒ focal modifier ⇒ slit filters ⇒ slit shutter ⇒ collimator ⇒ cross-dispersion prisms ⇒ echelle ⇒ CCD.

Calibration Lamps

A thorium-argon lamp is used to calibrate the instrument. This has an accompanying spectral atlas consisting of one long data file covering the wavelengths from 300.5 nm to 1 059.8 nm.

Image Slicer

A Bowen-Walraven image slicer consists of a stack of mirrors where light undergoes multiple total internal reflections. Light is allowed to escape after every second reflection.

CCD Detector

The EEV2 detector used a charge-coupled device (CCD). A CCD is a piece of doped silicon that produces electrons from light (photoelectric effect). The electrons accumulate in potential wells and the charge is read by coupling electrodes. The electric charge formed is proportional to the intensity of illumination (Kitchin 2003). This CCD contained 2 048 x 4 096 (2^{11} x 2^{12}) 13.5 µm square pixels with an image of 0.16 arcsecond per spatial pixel. The EEV2 device makes use of 2 048 x 2 746 pixels to reduce read-out time. In this operation 52 orders, numbered 80 to 131, can be recorded over the range 430-715 nm. The dispersion corresponds to a velocity measurement of 1.7 km s^{-1} $pixel^{-1}$. Details of the EEV2 CCD used (UCLES) are given in Table 2.1.

Table 2.1 Performance data of the EEV2 detector used (UCLES) with laboratory measurements in parentheses. Information is from the Anglo- Australian Observatory website http://www.aao.gov.au.

Speed	Read Out Time(s)	Gain (e-/ADU)	Read Out Noise (e-)	Saturation (e-)	Non-linearity (alpha x 10^{-6})
Slow	445 (403)	0.37	2.45 (2.3)	24 000 (ADC)	0.14
Normal	178 (158)	1.30	3.15 (3.2)	85 000 (ADC)	0.60
Fast	132 (132)	2.80	5.27 (5.35)	183 000 (ADC)	0.78
nonastro	89 (74)	6.67	9.74 (9.8)	437 000 (ADC)	1.92

Reduction of the CCD data includes flat fielding with the aid of a lamp used at the Cassegrain focus. A uniform source such as the Moon was used to check for zero polarisation to eliminate any effect due to the instrumentation (Kitchin 2003).

Cosmic rays can create problems with a CCD. This can be eliminated if one pixel registers too large a difference from those surrounding it. A correction can be applied by the software used (section 2.3) which replaces the value of this pixel with an average value derived from counts in the surrounding pixels (Kitchin 2003).

Variations may also occur due to background noise or due to pixel sensitivity differences which can be 10-20% over the whole area. Some pixels have permanently high levels referred to as hot spots. These may be replaced with the mean of four surrounding pixels. Also, cross talk refers to the straying of an electron from one pixel to another which can occur as the accumulating charge approaches the maximum capacity of the pixel which is 5×10^5 electrons for a 25 µm pixel (Kitchin 2003).

Observing Strategy

ZDI provides very small magnetic signatures so that every effort must be made to maximise signal and minimise noise. The use of a large telescope (3.893 m) to collect as much light as possible is the first necessity. Also, the target must have a satisfactory apparent brightness (AH Lep is magnitude 8.46).

However, this star is a rapid rotator ($v \sin i$ = 28 km s^{-1}) and a long exposure results in a smeared image. Semel et al. (1993) recommend an exposure for each collection to be in the order of 1-2 % of the rotation period of the star. 1 % of the 1.31 day period of AH Lep is 20 minutes.

Instrumentation has an effect on the image and the broadening of a spectral line due to the stellar rotation needs to be differentiated from that due to equipment.

In their work at the AAT Semel et al. (1993) and Donati et al. (2003a) use spectral resolutions of typically 70 000; this enables resolution of small-scale stellar features on moderately bright targets such as AH Lep.

For polarisation measurements the collection method of P1-P2-P2-P1 as mentioned under Semel Polarimeter allows a null method to cancel interference from

the instrument. Donati (2003) indicates that this procedure allows both beams to have a role exchange within the instrument to minimise spurious polarisation signatures.

Instrumental Setup

A more detailed and explanatory coverage of the instrumental setup is provided by Donati et al. (1997, 1999), Donati and Collier Cameron (1997), Donati (1999) and Donati et al. (2003a).

2.2 Observations at the AAT

Observations of AH Lep, called HD 36869 in the logs, were carried out beginning on the nights of 08, 09, 10 and 11 of December 2003 and much later on 10 and 11 of December 2008 at the AAT.

In the log for each night the instruments used shown at the top were a Semel Polarimeter fibre feed, UCLES and a CCD labelled EEV2. Then follows the family names of the observers. The columns from left to right give the number of the run, a file or star name, right ascension and declination both according to the J2000 epoch, Universal Time at the start of the run, the airmass which is defined as 1.000 for one atmosphere with the telescope pointed at the zenith and a larger amount at any other angle because of increased atmospheric content, the seeing which is given in arcseconds where a value of 1.5 is the median at this site, the time of exposure in seconds, the central wavelength in Å (5 267.97) and the grating (31). After two of the runs in 2003 comments on the cloud situation are given.

08 December 2003

Four runs form one set described previously with the Semel Polarimeter. On this occasion two sets were observed. The time for each run was 10 minutes (600 seconds). The sky had some cirrus clouds but seeing was 1.1″. The right ascension and declination figures for the telescope show some drift but images from the star are still captured.

09 December 2003

Two set of results were obtained each covering 10 minutes with 1.2″ seeing.

10 December 2003

Cloud and 1.5″ seeing accompanied the collection of one set of data on this evening.

11 December 2003

One set was collected with 10 minute exposures and 1.8″ seeing.

10 December 2008

On this occasion a set was taken that comprised 15 minute exposures under 1.6″ seeing.

11 December 2008

No data were obtained as the sky was totally covered in cloud.

Table 2.2 08 December 2003 Part of log of observations which include HD 36869 (AH Lep)

Anglo-Australian Observatory
UT Date : 2003-12-08 SEMEL POLARIMETER FIBRE FEED + UCLES + EEV2
Session : A Top End : F/8 Observers : SEMEL, DONATI, BARNES, MARSDEN

Run	Object	RA (J2000)	Dec (J2000)	UT start	Airmass	Seeing	Exposed	Wavelgth	Grating
1	BIAS_0001	00 00 00.00	+00 00 00.0	09:09:07.2	1.000	1.1	0.0	5267.97	31
2	BIAS_0002	00 00 00.00	+00 00 00.0	09:10:25.2	1.000	1.1	0.0	5267.97	31
3	BIAS_0003	00 00 00.00	+00 00 00.0	09:12:12.6	1.000	1.1	0.0	5267.97	31
4	BIAS_0004	00 00 00.00	+00 00 00.0	09:14:02.5	1.000	1.1	0.0	5267.97	31
5	BIAS_0005	00 00 00.00	+00 00 00.0	09:15:56.4	1.000	1.1	0.0	5267.97	31
6	BIAS_0006	00 00 00.00	+00 00 00.0	09:17:42.9	1.000	1.1	0.0	5267.97	31
7	BIAS_0007	00 00 00.00	+00 00 00.0	09:19:39.7	1.000	1.1	0.0	5267.97	31
8	BIAS_0008	00 00 00.00	+00 00 00.0	09:21:27.6	1.000	1.1	0.0	5267.97	31
9	BIAS_0009	00 00 00.00	+00 00 00.0	09:23:23.6	1.000	1.1	0.0	5267.97	31
10	BIAS_0010	00 00 00.00	+00 00 00.0	09:25:11.1	1.000	1.1	0.0	5267.97	31
11	flat	00 00 00.00	+00 00 00.0	09:27:38.3	1.000	1.1	6.0	5267.97	31
12	flat	00 00 00.00	+00 00 00.0	09:29:00.0	1.000	1.1	6.0	5267.97	31
13	flat	00 00 00.00	+00 00 00.0	09:31:01.2	1.000	1.1	6.0	5267.97	31
14	flat	00 00 00.00	+00 00 00.0	09:33:00.5	1.000	1.1	6.0	5267.97	31
15	flat	00 00 00.00	+00 00 00.0	09:34:53.4	1.000	1.1	6.0	5267.97	31
16	flat	00 00 00.00	+00 00 00.0	09:36:53.2	1.000	1.1	6.0	5267.97	31
17	flat	00 00 00.00	+00 00 00.0	09:38:44.1	1.000	1.1	6.0	5267.97	31
18	flat	00 00 00.00	+00 00 00.0	09:40:34.4	1.000	1.1	6.0	5267.97	31
19	flat	00 00 00.00	+00 00 00.0	09:42:25.6	1.000	1.1	6.0	5267.97	31
20	flat	00 00 00.00	+00 00 00.0	09:44:23.9	1.000	1.1	6.0	5267.97	31
21	fp	00 00 00.00	+00 00 00.0	09:46:37.6	1.000	1.1	30.0	5267.97	31
22	ThAr	00 41 46.17	-33 39 14.9	09:50:40.7	1.002	1.1	60.0	5267.97	31
23	ThAr	00 41 45.99	-33 39 14.4	09:52:58.8	1.002	1.1	60.0	5267.97	31
31	HD36869	05 34 09.22	-15 17 00.2	11:11:02.1	1.496	1.1	600.0	5267.97	31
31	Comment ********** some cirrus								
32	HD36869	05 34 09.24	-15 17 01.0	11:22:18.7	1.433	1.1	600.0	5267.97	31
32	Comment ********** some cirrus								
33	HD36869	05 34 09.24	-15 17 01.5	11:33:34.2	1.375	1.1	600.0	5267.97	31
33	Comment ********** some cirrus								
34	HD36869	05 34 09.07	-15 17 01.1	11:44:49.8	1.324	1.1	600.0	5267.97	31

34	Comment	**********	some cirrus									
35	HD36869		05	34	09.11	-15	17	01.4	11:56:05.6	1.281	1.1	600.0	5267.97	31
35	Comment	**********	some cirrus									
36	HD36869		05	34	09.18	-15	17	02.6	12:07:21.5	1.242	1.1	600.0	5267.97	31
36	Comment	**********	some cirrus									
37	HD36869		05	34	09.19	-15	17	01.6	12:18:38.3	1.207	1.1	600.0	5267.97	31
37	Comment	**********	some cirrus									
38	HD36869		05	34	09.27	-15	17	02.5	12:29:54.2	1.177	1.1	600.0	5267.97	31
38	Comment	**********	some cirrus									
39	Moon		04	43	11.33	+24	57	12.1	12:41:37.5	1.877	1.1	60.0	5267.97	31
83	ThAr		00	00	00.00	+00	00	00.0	18:22:22.3	1.481	1.1	60.0	5267.97	31
84	flat		00	00	00.00	+00	00	00.0	18:26:14.8	1.000	1.1	6.0	5267.97	31
85	flat		00	00	00.00	+00	00	00.0	18:31:54.6	1.000	1.1	6.0	5267.97	31
86	flat		00	00	00.00	+00	00	00.0	18:33:17.3	1.000	1.1	6.0	5267.97	31
87	flat		00	00	00.00	+00	00	00.0	18:35:01.6	1.000	1.1	6.0	5267.97	31
88	flat		00	00	00.00	+00	00	00.0	18:36:45.4	1.000	1.1	6.0	5267.97	31
89	flat		00	00	00.00	+00	00	00.0	18:38:42.3	1.000	1.1	6.0	5267.97	31
90	flat		00	00	00.00	+00	00	00.0	18:40:26.9	1.000	1.1	6.0	5267.97	31
91	flat		00	00	00.00	+00	00	00.0	18:42:21.2	1.000	1.1	6.0	5267.97	31
92	flat		00	00	00.00	+00	00	00.0	18:44:09.0	1.000	1.1	6.0	5267.97	31
93	flat		00	00	00.00	+00	00	00.0	18:45:51.4	1.000	1.1	6.0	5267.97	31
94	BIAS_0094		00	00	00.00	+00	00	00.0	18:50:35.4	1.000	1.1	0.0	5267.97	31
95	BIAS_0095		00	00	00.00	+00	00	00.0	18:51:54.2	1.000	1.1	0.0	5267.97	31
96	BIAS_0096		00	00	00.00	+00	00	00.0	18:53:38.1	1.000	1.1	0.0	5267.97	31
97	BIAS_0097		00	00	00.00	+00	00	00.0	18:55:24.8	1.000	1.1	0.0	5267.97	31
98	BIAS_0098		00	00	00.00	+00	00	00.0	18:57:03.4	1.000	1.1	0.0	5267.97	31
99	BIAS_0099		00	00	00.00	+00	00	00.0	18:58:58.7	1.000	1.1	0.0	5267.97	31
100	BIAS_0100		00	00	00.00	+00	00	00.0	19:00:45.6	1.000	1.1	0.0	5267.97	31
101	BIAS_0101		00	00	00.00	+00	00	00.0	19:02:44.1	1.000	1.1	0.0	5267.97	31
102	BIAS_0102		00	00	00.00	+00	00	00.0	19:04:31.5	1.000	1.1	0.0	5267.97	31
103	BIAS_0103		00	00	00.00	+00	00	00.0	19:06:27.5	1.000	1.1	0.0	5267.97	31

Table 2.3 09 December 2003 Part of log of observations which include HD 36869 (AH Lep)

Anglo-Australian Observatory
UT Date : 2003-12-09 SEMEL POLARIMETER FIBRE FEED + UCLES + EEV2
Session : A Top End : F/8 Observers : SEMEL, DONATI, BARNES, MARSDEN

Run	Object	RA (J2000)	Dec (J2000)	UT start	Airmass	Seeing	Exposed	Wavelgth	Grating
1	BIAS_0001	00 00 00.00	+00 00 00.0	09:12:23.9	1.000	1.2	0.0	5267.97	31
2	BIAS_0002	00 00 00.00	+00 00 00.0	09:13:41.2	1.000	1.2	0.0	5267.97	31
3	BIAS_0003	00 00 00.00	+00 00 00.0	09:15:29.9	1.000	1.2	0.0	5267.97	31
4	BIAS_0004	00 00 00.00	+00 00 00.0	09:17:23.2	1.000	1.2	0.0	5267.97	31
5	BIAS_0005	00 00 00.00	+00 00 00.0	09:19:12.1	1.000	1.2	0.0	5267.97	31
6	flat	00 00 00.00	+00 00 00.0	09:21:22.9	1.000	1.2	6.0	5267.97	31
7	flat	00 00 00.00	+00 00 00.0	09:23:54.4	1.000	1.2	6.0	5267.97	31
8	flat	00 00 00.00	+00 00 00.0	09:25:16.4	1.000	1.2	6.0	5267.97	31
9	flat	00 00 00.00	+00 00 00.0	09:27:09.2	1.000	1.2	6.0	5267.97	31
10	flat	00 00 00.00	+00 00 00.0	09:29:00.7	1.000	1.2	6.0	5267.97	31
11	fp	00 00 00.00	+00 00 00.0	09:31:17.9	1.000	1.2	30.0	5267.97	31
12	thar	00 00 00.00	+00 00 00.0	09:50:25.0	1.004	1.2	60.0	5267.97	31
13	thar	00 41 46.09	-33 39 13.4	09:52:41.5	1.003	1.2	60.0	5267.97	31
30	HD 36869	05 34 09.29	-15 17 01.0	11:18:57.2	1.428	1.2	600.0	5267.97	31
31	HD 36869	05 34 09.32	-15 17 00.5	11:30:13.6	1.373	1.2	600.0	5267.97	31
32	HD 36869	05 34 09.23	-15 17 01.0	11:41:29.1	1.322	1.2	600.0	5267.97	31
33	HD 36869	05 34 09.22	-15 17 02.4	11:52:46.5	1.279	1.2	600.0	5267.97	31
46	Moon	05 37 29.05	+27 04 00.0	13:56:36.7	1.931	1.2	60.0	5267.97	31
55	HD36869	05 34 09.18	-15 17 03.3	15:07:51.3	1.055	1.2	600.0	5267.97	31
56	HD36869	05 34 09.10	-15 17 03.0	15:19:06.7	1.064	1.2	600.0	5267.97	31
57	HD36869	05 34 09.07	-15 17 03.0	15:30:23.1	1.076	1.2	600.0	5267.97	31
58	HD36869	05 34 09.12	-15 17 03.1	15:41:38.3	1.090	1.2	600.0	5267.97	31
75	ThAr	05 28 44.63	-65 27 02.6	18:09:16.6	1.504	1.2	60.0	5267.97	31
76	BIAS_0076	08 41 32.07	-32 56 29.8	18:13:01.4	1.011	1.2	0.0	5267.97	31
77	BIAS_0077	00 00 00.00	+00 00 00.0	18:14:18.6	1.000	1.2	0.0	5267.97	31
78	BIAS_0078	00 00 00.00	+00 00 00.0	18:16:08.9	1.000	1.2	0.0	5267.97	31
79	BIAS_0079	00 00 00.00	+00 00 00.0	18:17:59.6	1.000	1.2	0.0	5267.97	31

80	BIAS_0080	00	00	00.00	+00	00	00.0	18:19:44.0	1.000	1.2	0.0	5267.97	31
81	flat	00	00	00.00	+00	00	00.0	18:21:53.2	1.000	1.2	6.0	5267.97	31
82	flat	00	00	00.00	+00	00	00.0	18:23:53.3	1.000	1.2	6.0	5267.97	31
83	flat	00	00	00.00	+00	00	00.0	18:25:20.7	1.000	1.2	6.0	5267.97	31
84	flat	00	00	00.00	+00	00	00.0	18:29:56.6	1.000	1.2	6.0	5267.97	31
85	flat	00	00	00.00	+00	00	00.0	18:31:18.2	1.000	1.2	6.0	5267.97	31
86	flat	00	00	00.00	+00	00	00.0	18:33:04.7	1.000	1.2	6.0	5267.97	31
87	flat	00	00	00.00	+00	00	00.0	18:35:00.9	1.000	1.2	6.0	5267.97	31
88	flat	00	00	00.00	+00	00	00.0	18:36:49.3	1.000	1.2	6.0	5267.97	31
89	flat	00	00	00.00	+00	00	00.0	18:38:40.3	1.000	1.2	6.0	5267.97	31
90	flat	00	00	00.00	+00	00	00.0	18:40:36.0	1.000	1.2	6.0	5267.97	31

Table 2.4 10 December 2003 Part of log of observations which include HD 36869 (AH Lep)

Anglo-Australian Observatory
UT Date : 2003-12-10 SEMEL POLARIMETER FIBRE FEED + UCLES + EEV2
Session : A Top End : F/8 Observers : SEMEL, DONATI, BARNES, MARSDEN

Run	Object			RA (J2000)	Dec (J2000)	UT start	Airmass	Seeing	Exposed	Wavelgth	Grating
1	BIAS_0001			00 00 00.00	+00 00 00.0	08:47:47.8	1.000	1.5	0.0	5267.97	31
2	BIAS_0002			00 00 00.00	+00 00 00.0	08:49:04.6	1.000	1.5	0.0	5267.97	31
3	BIAS_0003			00 00 00.00	+00 00 00.0	08:50:53.4	1.000	1.5	0.0	5267.97	31
4	BIAS_0004			00 00 00.00	+00 00 00.0	08:52:46.7	1.000	1.5	0.0	5267.97	31
5	BIAS_0005			00 00 00.00	+00 00 00.0	08:54:35.3	1.000	1.5	0.0	5267.97	31
6	flat			00 00 00.00	+00 00 00.0	09:04:55.5	1.000	1.5	8.0	5267.97	31
7	flat			00 00 00.00	+00 00 00.0	09:07:07.4	1.000	1.5	10.0	5267.97	31
8	flat			00 00 00.00	+00 00 00.0	09:09:19.0	1.000	1.5	10.0	5267.97	31
9	flat			00 00 00.00	+00 00 00.0	09:10:45.0	1.000	1.5	10.0	5267.97	31
10	flat			00 00 00.00	+00 00 00.0	09:12:39.4	1.000	1.5	10.0	5267.97	31
11	flat			00 00 00.00	+00 00 00.0	09:14:33.5	1.000	1.5	10.0	5267.97	31
12	flat			00 00 00.00	+00 00 00.0	09:16:27.8	1.000	1.5	10.0	5267.97	31
13	flat			00 00 00.00	+00 00 00.0	09:18:22.4	1.000	1.5	10.0	5267.97	31
14	flat			00 00 00.00	+00 00 00.0	09:20:17.1	1.000	1.5	10.0	5267.97	31
15	flat			00 00 00.00	+00 00 00.0	09:22:10.3	1.000	1.5	10.0	5267.97	31
16	flat			00 00 00.00	+00 00 00.0	09:24:03.2	1.000	1.5	10.0	5267.97	31
17	fp			00 00 00.00	+00 00 00.0	09:26:20.0	1.000	1.5	30.0	5267.97	31
18	ThAr			00 00 00.00	+00 00 00.0	09:30:29.9	1.000	1.5	60.0	5267.97	31
19	ThAr			00 41 29.76	-20 17 57.3	09:32:49.1	1.019	1.5	60.0	5267.97	31
20	HD36869			05 34 09.13	-15 16 58.8	09:45:03.0	2.348	1.5	600.0	5267.97	31
20	Comment	**********	cloud								
21	HD36869			05 34 09.03	-15 16 59.8	09:56:19.4	2.151	1.5	600.0	5267.97	31
21	Comment	**********	cloud								
22	HD36869			05 34 09.03	-15 17 00.3	10:07:35.6	1.994	1.5	600.0	5267.97	31
22	Comment	**********	cloud								
23	HD36869			05 34 09.07	-15 17 00.7	10:18:51.2	1.862	1.5	600.0	5267.97	31
23	Comment	**********	cloud								
68	Moon			06 31 46.90	+27 48 31.5	14:01:08.1	2.123	1.5	60.0	5267.97	31
93	thar			00 00 00.00	+00 00 00.0	16:44:12.1	1.012	1.5	60.0	5267.97	31

94	thar	00 00 00.00	+00 00 00.0	16:46:27.5	1.000	1.5	60.0	5267.97	31
95	flat	00 00 00.00	+00 00 00.0	16:51:41.7	1.000	1.5	10.0	5267.97	31
96	flat	00 00 00.00	+00 00 00.0	16:55:40.6	1.000	1.5	10.0	5267.97	31
97	flat	00 00 00.00	+00 00 00.0	16:58:01.7	1.000	1.5	8.0	5267.97	31
98	flat	00 00 00.00	+00 00 00.0	17:00:10.9	1.000	1.5	8.0	5267.97	31
99	flat	00 00 00.00	+00 00 00.0	17:01:34.5	1.000	1.5	8.0	5267.97	31
100	flat	00 00 00.00	+00 00 00.0	17:03:29.4	1.000	1.5	8.0	5267.97	31
101	flat	00 00 00.00	+00 00 00.0	17:05:24.2	1.000	1.5	8.0	5267.97	31
102	flat	00 00 00.00	+00 00 00.0	17:07:19.3	1.000	1.5	8.0	5267.97	31
103	flat	00 00 00.00	+00 00 00.0	17:09:13.6	1.000	1.5	8.0	5267.97	31
104	flat	00 00 00.00	+00 00 00.0	17:11:07.5	1.000	1.5	8.0	5267.97	31
105	flat	00 00 00.00	+00 00 00.0	17:13:01.2	1.000	1.5	8.0	5267.97	31
106	flat	00 00 00.00	+00 00 00.0	17:14:56.0	1.000	1.5	8.0	5267.97	31
107	fp	00 00 00.00	+00 00 00.0	17:18:18.7	1.000	1.5	30.0	5267.97	31
108	BIAS_0108	00 00 00.00	+00 00 00.0	17:22:37.0	1.000	1.5	0.0	5267.97	31
109	BIAS_0109	00 00 00.00	+00 00 00.0	17:23:54.6	1.000	1.5	0.0	5267.97	31
110	BIAS_0110	00 00 00.00	+00 00 00.0	17:25:43.9	1.000	1.5	0.0	5267.97	31
111	BIAS_0111	00 00 00.00	+00 00 00.0	17:27:34.9	1.000	1.5	0.0	5267.97	31
112	BIAS_0112	00 00 00.00	+00 00 00.0	17:29:23.5	1.000	1.5	0.0	5267.97	31
113	BIAS_0113	00 00 00.00	+00 00 00.0	17:31:13.6	1.000	1.5	0.0	5267.97	31
114	BIAS_0114	00 00 00.00	+00 00 00.0	17:33:02.5	1.000	1.5	0.0	5267.97	31
115	BIAS_0115	00 00 00.00	+00 00 00.0	17:34:52.9	1.000	1.5	0.0	5267.97	31
116	BIAS_0116	00 00 00.00	+00 00 00.0	17:36:42.0	1.000	1.5	0.0	5267.97	31
117	BIAS_0117	00 00 00.00	+00 00 00.0	17:38:32.6	1.000	1.5	0.0	5267.97	31

Table 2.5 11 December 2003 Part of log of observations which include HD 36869 (AH Lep)

Anglo-Australian Observatory
UT Date : 2003-12-11 SEMEL POLARIMETER FIBRE FEED + UCLES + EEV2
Session : A Top End : F/8 Observers : SEMEL, (DONATI, BARNES), MARSDEN, CARTER

Run	Object	RA (J2000)	Dec (J2000)	UT start	Airmass	Seeing	Exposed	Wavelgth	Grating
1	BIAS_0001	00 00 00.00	+00 00 00.0	09:03:22.6	1.000		0.0	5267.97	31
2	BIAS_0002	00 00 00.00	+00 00 00.0	09:04:40.2	1.000		0.0	5267.97	31
3	BIAS_0003	00 00 00.00	+00 00 00.0	09:06:27.5	1.000		0.0	5267.97	31
4	BIAS_0004	00 00 00.00	+00 00 00.0	09:08:17.8	1.000		0.0	5267.97	31
5	BIAS_0005	00 00 00.00	+00 00 00.0	09:10:06.8	1.000		0.0	5267.97	31
6	flat	00 00 00.00	+00 00 00.0	09:13:36.0	1.000		8.0	5267.97	31
7	flat	00 00 00.00	+00 00 00.0	09:15:39.8	1.000		8.0	5267.97	31
8	flat	00 00 00.00	+00 00 00.0	09:17:03.5	1.000		8.0	5267.97	31
9	flat	00 00 00.00	+00 00 00.0	09:18:50.2	1.000		8.0	5267.97	31
10	flat	00 00 00.00	+00 00 00.0	09:20:31.3	1.000		8.0	5267.97	31
11	flat	00 00 00.00	+00 00 00.0	09:22:19.0	1.000		8.0	5267.97	31
12	flat	00 00 00.00	+00 00 00.0	09:24:03.2	1.000		8.0	5267.97	31
13	flat	00 00 00.00	+00 00 00.0	09:25:45.0	1.000		8.0	5267.97	31
14	flat	00 00 00.00	+00 00 00.0	09:27:31.9	1.000		8.0	5267.97	31
15	flat	00 00 00.00	+00 00 00.0	09:29:14.2	1.000		8.0	5267.97	31
16	fp	00 00 00.00	+00 00 00.0	09:32:13.9	1.000		30.0	5267.97	31
17	thar	00 00 00.00	+00 00 00.0	09:35:29.3	1.000		60.0	5267.97	31
18	thar	00 00 00.00	+00 00 00.0	09:37:45.5	1.000		60.0	5267.97	31
19	HD 36869	05 34 09.07	-15 17 00.2	10:08:30.8	1.937	1.8	600.0	5267.97	31
20	HD 36869	05 34 09.11	-15 17 00.6	10:19:49.4	1.813	1.8	600.0	5267.97	31
21	HD 36869	05 34 09.06	-15 17 02.1	10:31:05.9	1.702	1.8	600.0	5267.97	31
22	HD 36869	05 34 08.99	-15 17 01.9	10:42:22.0	1.611	1.8	600.0	5267.97	31
44	Thar	00 00 00.00	+00 00 00.0	14:21:24.0	1.000		60.0	5267.97	31
45	BIAS_0045	00 00 00.00	+00 00 00.0	14:24:27.7	1.000		0.0	5267.97	31
46	BIAS_0046	00 00 00.00	+00 00 00.0	14:25:45.8	1.000		0.0	5267.97	31
47	BIAS_0047	00 00 00.00	+00 00 00.0	14:27:34.6	1.000		0.0	5267.97	31
48	BIAS_0048	00 00 00.00	+00 00 00.0	14:29:25.0	1.000		0.0	5267.97	31
49	BIAS_0049	00 00 00.00	+00 00 00.0	14:31:10.1	1.000		0.0	5267.97	31
50	flat	00 00 00.00	+00 00 00.0	17:41:30.6	1.000		8.0	5267.97	31

51	flat	00 00 00.00	+00 00 00.0	17:43:38.3	1.000		8.0	5267.97	31
52	flat	00 00 00.00	+00 00 00.0	17:45:02.4	1.000		8.0	5267.97	31
53	flat	00 00 00.00	+00 00 00.0	17:46:56.3	1.000		8.0	5267.97	31
54	flat	00 00 00.00	+00 00 00.0	17:48:50.4	1.000		8.0	5267.97	31
55	flat	00 00 00.00	+00 00 00.0	17:50:44.3	1.000		8.0	5267.97	31
56	flat	00 00 00.00	+00 00 00.0	17:52:38.6	1.000		8.0	5267.97	31
57	flat	00 00 00.00	+00 00 00.0	17:54:31.3	1.000		8.0	5267.97	31
58	flat	00 00 00.00	+00 00 00.0	17:56:19.7	1.000		8.0	5267.97	31
59	flat	00 00 00.00	+00 00 00.0	17:58:14.2	1.000		8.0	5267.97	31

Table 2.6 10 December 2008 Part of log of observations which include HD 36869 (AH Lep)

Anglo-Australian Observatory
UT Date : 2008-12-10 SEMEL POLARIMETER FIBRE FEED + UCLES + EEV2
Session : A Top End : F/8 Observers : MARSDEN, WAITE, GUGGENBERGER, CARTER, TRESCHMAN (BURTON, ET AL)

Run	Object	RA (J2000)	Dec (J2000)	UT start	Airmass	Seeing	Exposed	Wavelgth	Grating
1	flat	23 34 37.94	-31 19 29.0	08:21:08	1.000		3.0	5268.00	31
2	flat	23 36 05.42	-31 19 29.1	08:22:35	1.000		3.0	5268.00	31
3	flat	23 37 32.81	-31 19 29.3	08:24:02	1.000		3.0	5268.00	31
4	flat	23 39 00.23	-31 19 29.4	08:25:29	1.000		3.0	5268.00	31
5	flat	23 40 27.49	-31 19 29.6	08:26:56	1.000		3.0	5268.00	31
6	flat	23 41 54.84	-31 19 29.7	08:28:23	1.000		3.0	5268.00	31
7	flat	23 43 22.21	-31 19 29.9	08:29:50	1.000		3.0	5268.00	31
8	flat	23 44 49.51	-31 19 30.0	08:31:17	1.000		3.0	5268.00	31
9	flat	23 46 17.01	-31 19 30.3	08:32:45	1.000		3.0	5268.00	31
10	flat	23 47 44.63	-31 19 30.3	08:34:12	1.000		3.0	5268.00	31
11	fabp	23 50 22.40	-31 19 30.5	08:36:49	1.000		30.0	5268.00	31
12	fabp	23 52 16.93	-31 19 30.6	08:38:43	1.000		30.0	5268.00	31
13	bias	23 57 03.94	-31 19 30.9	08:43:29	1.000		0.0	5268.00	31
14	bias	23 58 28.40	-31 19 30.9	08:44:53	1.000		0.0	5268.00	31
15	bias	23 59 52.63	-31 19 31.0	08:46:17	1.000		0.0	5268.00	31
16	bias	00 01 17.01	-31 19 31.0	08:47:41	1.000		0.0	5268.00	31
17	bias	00 02 41.35	-31 19 31.1	08:49:06	1.000		0.0	5268.00	31
18	bias	00 04 05.58	-31 19 31.1	08:50:30	1.000		0.0	5268.00	31
19	bias	00 05 29.91	-31 19 31.1	08:51:54	1.000		0.0	5268.00	31
20	bias	00 06 54.33	-31 19 31.1	08:53:18	1.000		0.0	5268.00	31
21	bias	00 08 18.89	-31 19 31.1	08:54:42	1.000		0.0	5268.00	31
22	bias	00 09 43.21	-31 19 31.2	08:56:06	1.000		0.0	5268.00	31
23	flat	00 49 40.10	-31 19 29.4	09:35:55	1.000		4.0	5268.00	31
24	fabp	00 51 36.27	-31 19 29.2	09:37:51	1.000		30.0	5268.00	31
25	bias	00 53 57.65	-31 19 28.9	09:40:12	1.000		0.0	5268.00	31
26	thar	21 20 48.43	-53 02 02.9	09:47:19	1.408		60.0	5268.00	31
51	HD36869	05 34 08.54	-15 17 02.9	14:55:03	1.051	1.6	900.0	5268.00	31
52	HD36869	05 34 08.55	-15 17 03.7	15:11:31	1.063	1.6	900.0	5268.00	31
53	HD36869	05 34 08.41	-15 17 03.5	15:27:58	1.081	1.6	900.0	5268.00	31
54	HD36869	05 34 08.58	-15 17 03.8	15:44:26	1.105	1.6	900.0	5268.00	31

68	thar	09	56	35.32	-31	14	15.1	18:41:18	1.000	1.6	60.0	5268.00	31
69	thar	09	59	03.70	-31	14	14.0	18:43:46	1.000	1.6	60.0	5268.00	31
70	flat	10	08	06.02	-31	14	10.5	18:52:47	1.000	1.6	3.0	5268.00	31
71	flat	10	09	33.45	-31	14	09.9	18:54:14	1.000	1.6	3.0	5268.00	31
72	flat	10	11	00.67	-31	14	09.3	18:55:41	1.000	1.6	3.0	5268.00	31
73	flat	10	12	27.91	-31	14	08.8	18:57:08	1.000	1.6	3.0	5268.00	31
74	flat	10	13	55.19	-31	14	08.3	18:58:35	1.000	1.6	3.0	5268.00	31
75	flat	10	15	22.52	-31	14	07.8	19:00:02	1.000	1.6	3.0	5268.00	31
76	flat	10	16	49.88	-31	14	07.3	19:01:29	1.000	1.6	3.0	5268.00	31
77	flat	10	18	17.19	-31	14	06.7	19:02:56	1.000	1.6	3.0	5268.00	31
78	flat	10	19	44.29	-31	14	06.2	19:04:23	1.000	1.6	3.0	5268.00	31
79	flat	10	21	11.62	-31	14	05.7	19:05:50	1.000	1.6	3.0	5268.00	31
80	flat	10	22	39.98	-31	14	05.3	19:07:18	1.000	1.6	3.0	5268.00	31
81	flat	10	24	07.13	-31	14	04.8	19:08:45	1.000	1.6	3.0	5268.00	31
82	flat	10	25	34.38	-31	14	04.3	19:10:12	1.000	1.6	3.0	5268.00	31
83	flat	10	27	01.63	-31	14	03.8	19:11:40	1.000	1.6	3.0	5268.00	31
84	flat	10	28	28.94	-31	14	03.3	19:13:07	1.000	1.6	3.0	5268.00	31
85	flat	10	29	56.44	-31	14	02.9	19:14:34	1.000	1.6	3.0	5268.00	31
86	flat	10	31	23.69	-31	14	02.4	19:16:01	1.000	1.6	3.0	5268.00	31
87	flat	10	32	51.03	-31	14	02.0	19:17:28	1.000	1.6	3.0	5268.00	31
88	flat	10	34	18.33	-31	14	01.5	19:18:55	1.000	1.6	3.0	5268.00	31
89	flat	10	35	45.68	-31	14	01.1	19:20:22	1.000	1.6	3.0	5268.00	31
90	fabp	10	37	32.10	-31	14	00.5	19:22:08	1.000	1.6	30.0	5268.00	31
91	fabp	10	39	26.51	-31	14	00.0	19:24:03	1.000	1.6	30.0	5268.00	31
92	bias	10	42	32.86	-31	13	58.7	19:27:08	1.000	1.6	0.0	5268.00	31
93	bias	10	43	57.22	-31	13	58.0	19:28:33	1.000	1.6	0.0	5268.00	31
94	bias	10	45	21.53	-31	13	57.6	19:29:57	1.000	1.6	0.0	5268.00	31
95	bias	10	46	45.80	-31	13	57.1	19:31:21	1.000	1.6	0.0	5268.00	31
96	bias	10	48	10.07	-31	13	56.7	19:32:45	1.000	1.6	0.0	5268.00	31
97	bias	10	49	34.40	-31	13	56.3	19:34:09	1.000	1.6	0.0	5268.00	31
98	bias	10	51	00.92	-31	13	56.0	19:35:35	1.000	1.6	0.0	5268.00	31
99	bias	10	52	25.16	-31	13	55.6	19:36:59	1.000	1.6	0.0	5268.00	31
100	bias	10	53	49.46	-31	13	55.2	19:38:24	1.000	1.6	0.0	5268.00	31
101	bias	10	55	13.71	-31	13	54.9	19:39:48	1.000	1.6	0.0	5268.00	31
102	bias	10	56	37.87	-31	13	54.5	19:41:12	1.000	1.6	0.0	5268.00	31
103	bias	10	58	02.19	-31	13	54.2	19:42:36	1.000	1.6	0.0	5268.00	31
104	bias	10	59	26.52	-31	13	53.8	19:44:00	1.000	1.6	0.0	5268.00	31
105	bias	11	00	50.65	-31	13	53.5	19:45:24	1.000	1.6	0.0	5268.00	31

106	bias	11 02 14.87	-31 13 53.2	19:46:48	1.000	1.6	0.0	5268.00	31
107	bias	11 03 39.20	-31 13 52.9	19:48:12	1.000	1.6	0.0	5268.00	31
108	bias	11 05 03.52	-31 13 52.6	19:49:36	1.000	1.6	0.0	5268.00	31
109	bias	11 06 27.85	-31 13 52.3	19:51:00	1.000	1.6	0.0	5268.00	31
110	bias	11 07 51.97	-31 13 52.0	19:52:24	1.000	1.6	0.0	5268.00	31
111	bias	11 09 16.25	-31 13 51.7	19:53:48	1.000	1.6	0.0	5268.00	31

2.3 Analysis

The reshaping of lines in the spectrum due to the magnetic field is a very small effect. The strategy is to consider that this change to a line will have the same basis in all lines. So, instead of looking at one line, thousands of lines are combined. The result is that the detection is now measurable. Jean-Francois Donati (Donati 1997) has produced a custom package for Doppler Imaging and ZDI. It is known as ESpRIT for *E*chelle *Sp*ectra *R*eduction: an *I*nteractive *T*ool. There are six steps in the analysis.

2.3.1 Geometry Correction

In the operation of the Bowen-Walraven image slicer the image is produced in strips side by side with the data being trimmed to the appropriate size. Some distortion also occurs due to the projection of the slit shape at different wavelengths so the geometrical shape, that is, the curvature of the orders is measured. A fit to bias values averaged on a box of eight pixels by eight pixels is subtracted. The CCD frame needs to be examined for hot spots or pixels which are recording differently from their surroundings.

Prior to and after the observations a lamp on a stick is placed in front of the fibre feed with a diffuser to correct for any nonuniformity in the illumination and detector. This is called a flat field operation. Any bias is accounted for in the analysis. Moonlight is used to correct for any polarisation due to the instrument and to determine the contribution from absorption of the gases in the atmosphere of the Earth, such as oxygen, water vapour and carbon dioxide. These chemicals produce several telluric lines in the spectrum.

Input to the package includes information that dispersion is along the columns and that wavelength decreases with the pixels along the orders. The row number at the centre point of the first order is determined by eye and the pixel number in that row is noted. The separation between the orders in terms of pixel numbers needs to be ascertained. The number of the first order is noted along with the information that the order increments towards the top of the CCD. The correction tool is fed the maximum number of orders along with a request to correct for slit curvature.

2.3.2 Wavelength Calibration

Light from a thorium-argon arc lamp is used to establish a wavelength scale. Two established lines from the lamp were recorded and subtraction of wavelengths and pixel numbers gives dispersion in nm per pixel. ESpIRIT uses a polynomial applied to the wavelength to compensate for non-linearity in the spectra. Thus, the position on a pixel can be given a wavelength for the entire spectrum.

2.3.3 Extraction of Spectra

Extraction of spectra takes two forms: intensity and polarisation.

For intensity analysis all the frames have any bias subtracted and a correction is made for differences in sensitivity between pixels by comparison with the relevant pixels when exposed to the flat field. Cosmic ray bombardment is responsible for some pixel measurements deviating from the average intensity of the order. These are discarded if they are beyond a set threshold.

The polarisation extraction is similar to the intensity one. Four runs of records exist in each set in the sequence P1-P2-P2-P1 where P1 measures right-handed polarisation and P2 left. Thus, P1 is 90˚ to P2.

Since I, $I + V$ and $I - V$ are measured, a null arrangement can deduce the contribution of V. The output of this step is a probability that a magnetic field has been detected.

2.3.4 Least Squares Deconvolution

While typical variations of amplitude in the intensity (1%) and magnetic (0.1%) signatures are very small, this method rests on the assumption that any distortion in one line is approximately replicated across all lines. Thus, the tiny effect is compounded across thousands of lines to produce a detectable signal. There is some overlap in orders in the echelle spectrograph so the redundancy is used by the program. The aim is to produce a high signal-to-noise ratio for both the intensity and magnetic data.

The technique of summing these differences is called Least Squares Deconvolution (LSD) by Donati et al. (1997). There would be many solutions of magnetic

fields which would match the data. The selected magnetic field along a three dimensional axis is derived by making use of an iterative reconstruction based on a least squares compilation.

2.3.5 Reformatting of Line Profile Data

This step takes the data from the previous step and rearranges them into a form suitable for the imaging codes in the next step. It is also able to combine any data from photometry that has been obtained for that particular star.

2.3.6 Imaging

An imaging code selects via an algorithm for maximum entropy reconstruction the minimum spot features that would produce the observed spectroscopic features. A reconstruction is built based on the contribution of each pixel to a cool spot on the surface of the star. The photosphere and spots are matched against the profiles of slowly-rotating stars. In the mapping of brightness a filling factor is used. This is based on 0 for no spot and 1 for a total spot convergence (Collier Cameron 1992). The data are fitted to the desired accuracy, that is, usually to the level of noise.

If the star has been observed over several rotations, a magnetic map may also be compiled (Donati and Brown 1997). The operation is similar to the technique used for the brightness image. In the matching assumptions are that the magnetic fields are weak and that there are areas of constancy across the stellar surface. The result is a series of images based on the three dimensional aspect of the magnetic field, namely components in the radial, azimuthal and meridional directions.

Chapter 3 Results and Discussion

3.1 Magnetic Field Detection on AH Lep

The surface topology of a star may be ascertained with the technique outlined here with a number of basic stellar parameters. The temperature of the photosphere was calculated in equation 4 and the temperature of the spots is cooler. The radial velocity measurement from literature is checked with a χ^2 minimisation technique in Figure 3.5 later. This procedure is also used in Figure 3.4 later for determining the radial velocity. Once this is obtained, the inclination of the rotational axis of the star is determined from the period and the radius as in equation 10.

For the four nights of observations in December 2003 two cycles were conducted on each of 08 and 09 and one each on 10 and 11. In December 2008 one further cycle was recorded on 10 and no data were possible on 11 due to unfavourable weather conditions.

The instrumental setup has been described in Chapter 2 and ESpRIT was used for data reduction. Intensity profiles and magnetic signatures were analysed from the compilation of over 2 600 spectral lines used in the calculation for each case. The software delivers a decision on whether a magnetic detection occurred in terms of a false alarm probability. This output is given in Table 3.1.

Table 3.1 False alarm probabilities for magnetic detection for each cycle of data sets gathered on five nights with around 10^{-6} a threshold for definite detection.

Date	False Alarm Probability
2003 Dec 08 cycle 1	3.226×10^{-1}
2003 Dec 08 cycle 2	4.393×10^{-6}
2003 Dec 09 cycle 1	2.460×10^{-1}
2003 Dec 09 cycle 2	4.104×10^{-3}
2003 Dec 10	3.407×10^{-1}
2003 Dec 11	4.451×10^{-1}
2008 Dec 10	1.065×10^{-12}

A definite detection is described for 2003 December 08 cycle 2 and 2008 December 10 with a marginal one reported for 2003 December 09 cycle 2. The profiles for these detections are shown in Figures 3.1, 3.2 and 3.3. The flat section in the trough of the Stokes I profile is a characteristic of stars that display a reasonable degree of spot features.

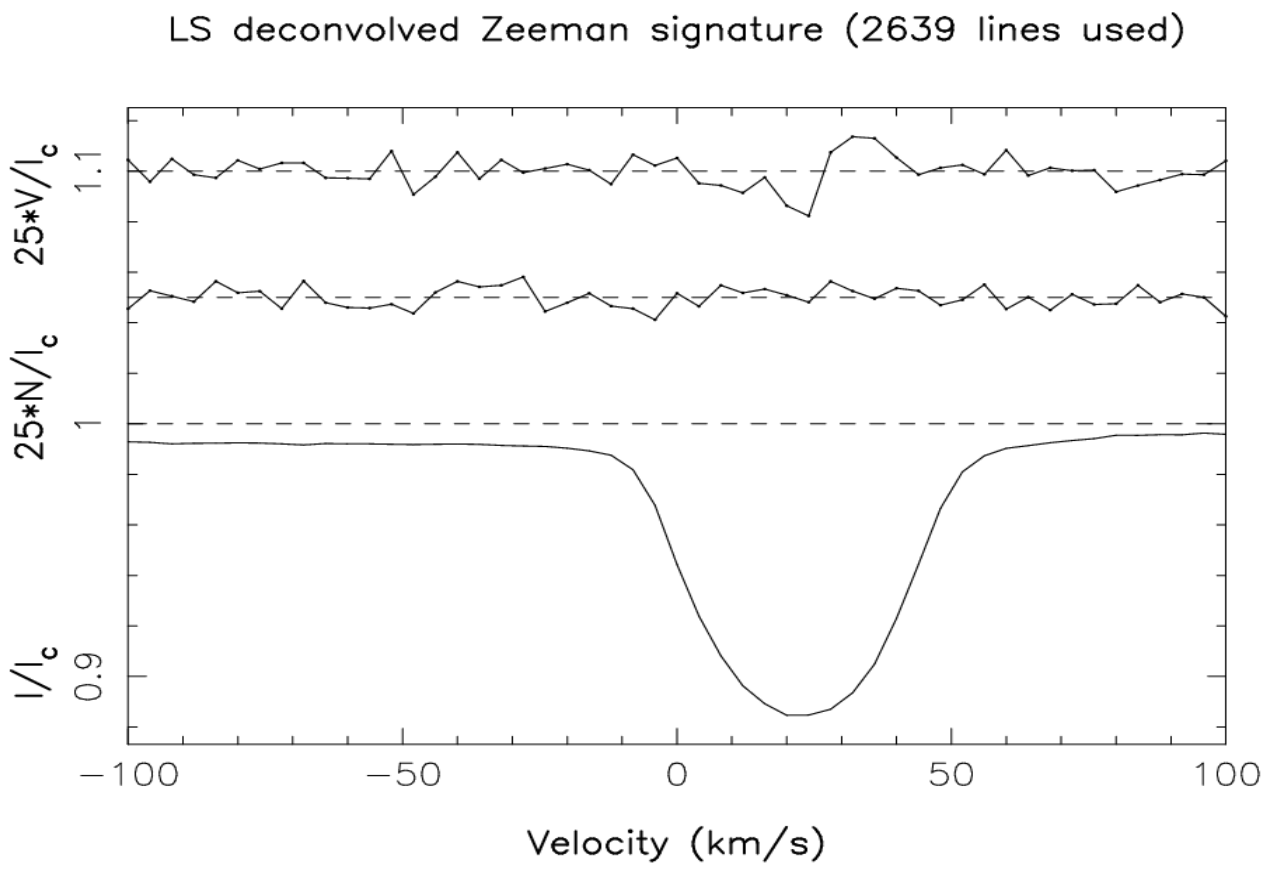

Figure 3.1 Detection of magnetic field on AH Lep on 08 December 2003 cycle 2. The top line is the magnetic signature (Stokes *V* profile), the central line the null polarisation profile and the lower line is the intensity profile (Stokes I). The *V* and *N* profiles have been multiplied by 25 and shifted upwards to separate the three plots.

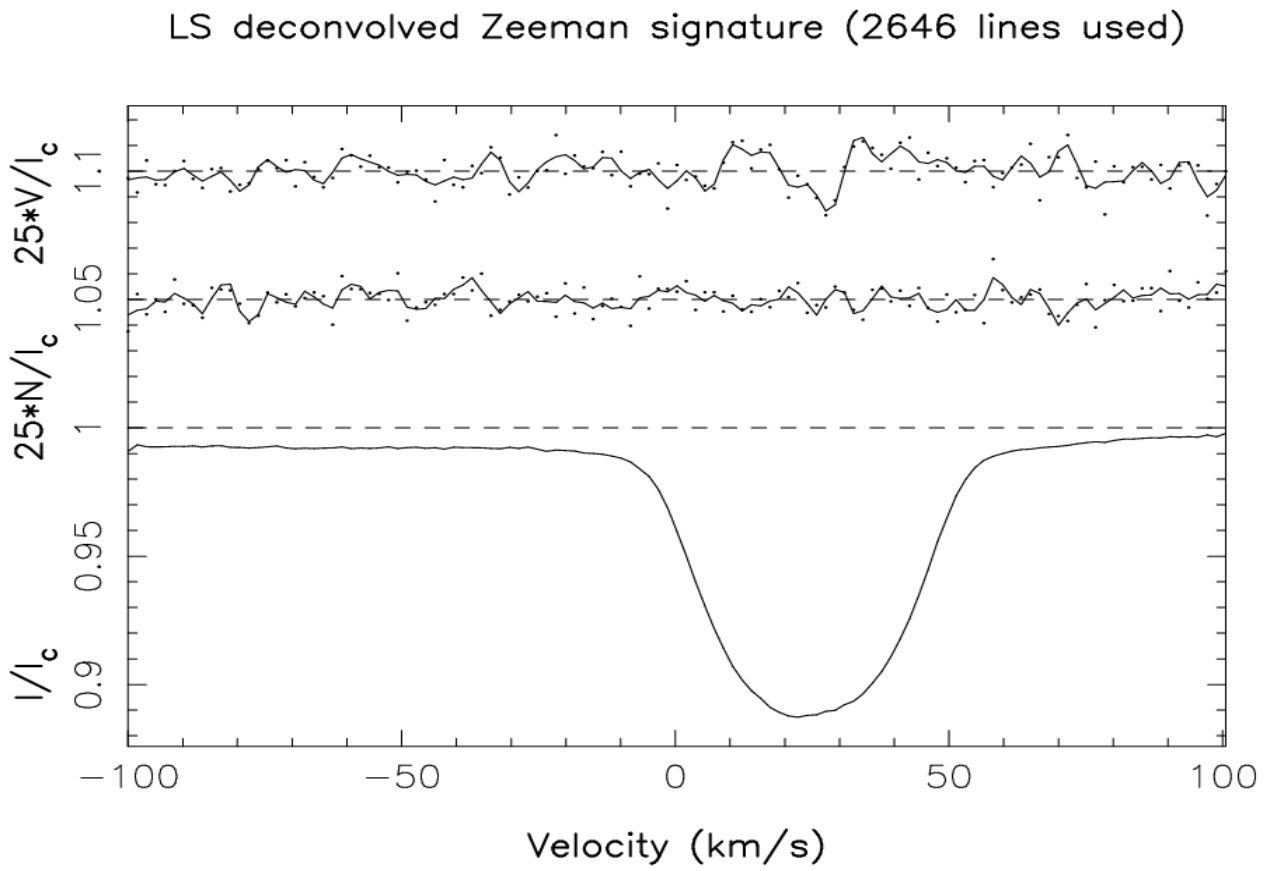

Figure 3.2 Detection of magnetic field on AH Lep on 09 December 2003 cycle 2. The top line is the Stokes *V* magnetic profile, the central line the null polarisation profile and the lower line is the Stokes I intensity profile. The *V* and *N* profiles have been multiplied by 25 and shifted upwards for clarity. The dots represent data points for which smoothing curves are drawn. The absence of such dots in Figure 3.1 represents an excellent fit.

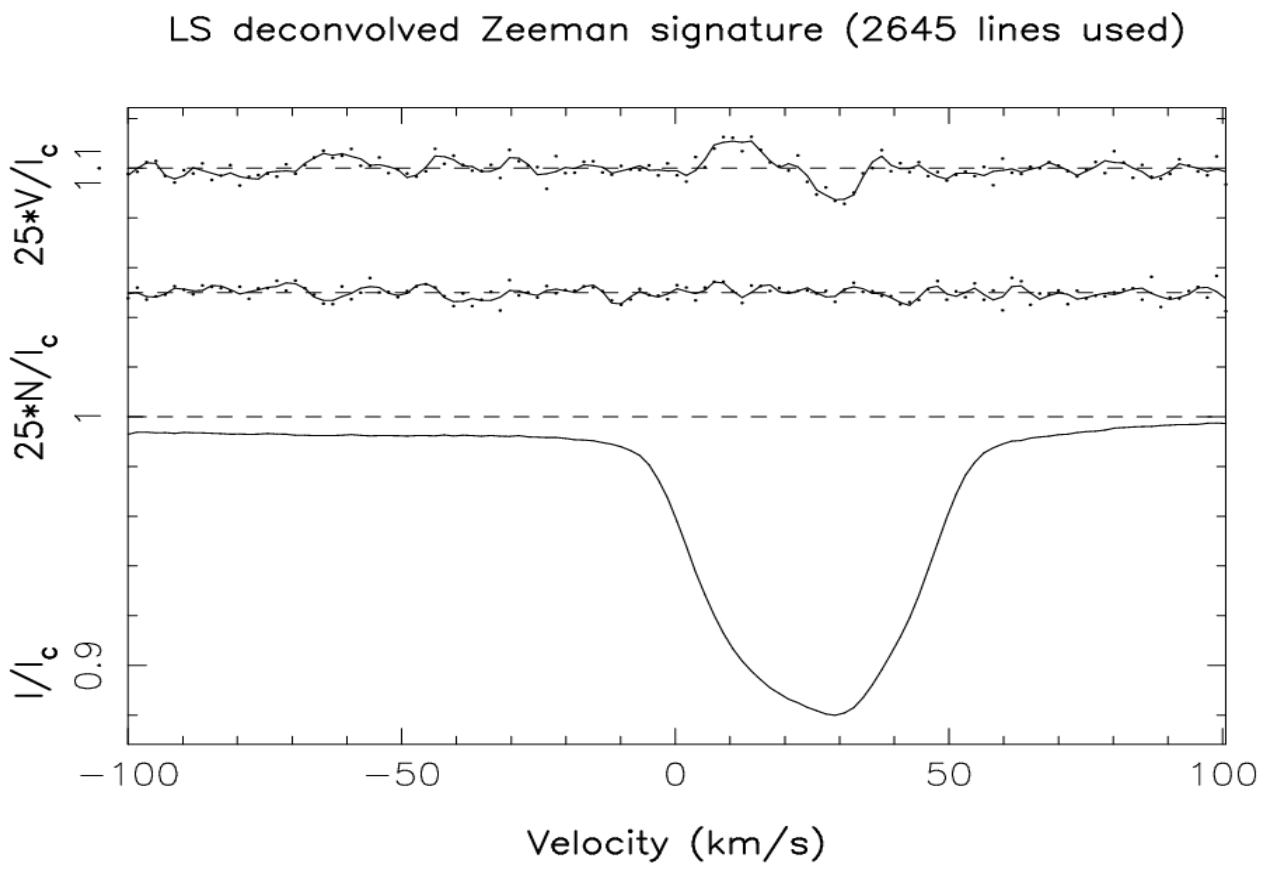

Figure 3.3 Detection of magnetic field on AH Lep on 10 December 2008. The top line is the magnetic signature (Stokes *V* profile), the central line the null polarisation profile and the lower line is the intensity profile (Stokes I). The *V* and *N* profiles have been multiplied by 25 and shifted upwards for clarity. The dots represent data points for which smoothing curves are drawn.

3.2 Radial Velocity of AH Lep

The Stokes I profile is offset from 0 km s^{-1} due to the radial velocity of the star. A preliminary range of 23-30 km s^{-1} is obtained from the preceding three graphs. However, a χ^2minimisation technique can be applied to the data to refine the radial velocity. The figures analysed are shown in Table 3.2 and graphed in Figure 3.4.

Table 3.2 χ^2 values for a range of radial velocity figures for AH Lep.

Radial Velocity in km s^{-1}	24.0	24.3	24.4	24.5	24.6	24.7	24.8	24.9	25.0	26.0
Chi Squared	2.02	1.21	1.07	1.00	1.02	1.11	1.26	1.39	1.59	9.15

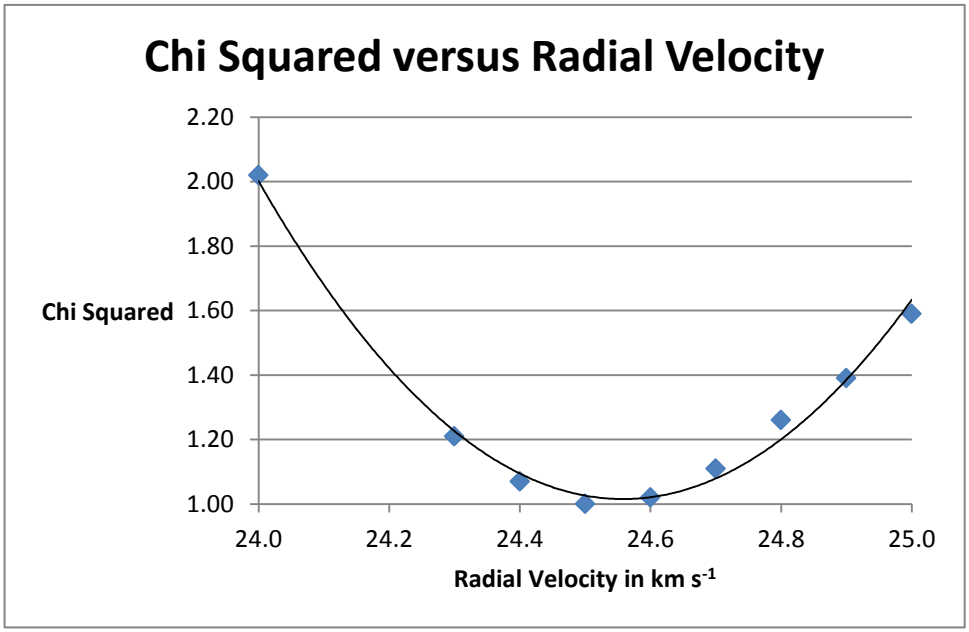

Figure 3.4 Graph of χ2 versus radial velocity for AH Lep with the extreme datum of 26 km s^{-1} excluded due to its very large chi squared value).

From observation of the graph the radial velocity is determined as 24.5 km s^{-1}. Analysis gives one standard deviation as 2.0 km s^{-1}. This result is consistent with that of Montes et al. (2001) of 24.1 ± 2.0 km s^{-1} and Wichmann et al. (2003) of 24.9 ± 2-3 km s^{-1}.

3.3 Results of Doppler Imaging of AH Lep

V sin *i* is given as 30 km s^{-1} by Wickmann et al. (2003) and Cutispoto et al. (2003b) and 28 km s^{-1} by Montes et al. (2001) and Messina et al. (2001). Again, a χ^2minimisation technique can be applied to the data to refine the value of *v* sin *i.* The figures analysed are shown in Table 3.3 and graphed in Figure 3.5.

Table 3.3 χ^2 values for a range of *v* sin *i* figures for AH Lep.

v sin *i* in km s^{-1}	27.4	27.5	27.6	27.7	27.8	27.9	28.0	28.1	28.2
Chi Squared	0.637	0.504	0.239	0.209	0.176	0.143	0.108	0.164	0.208

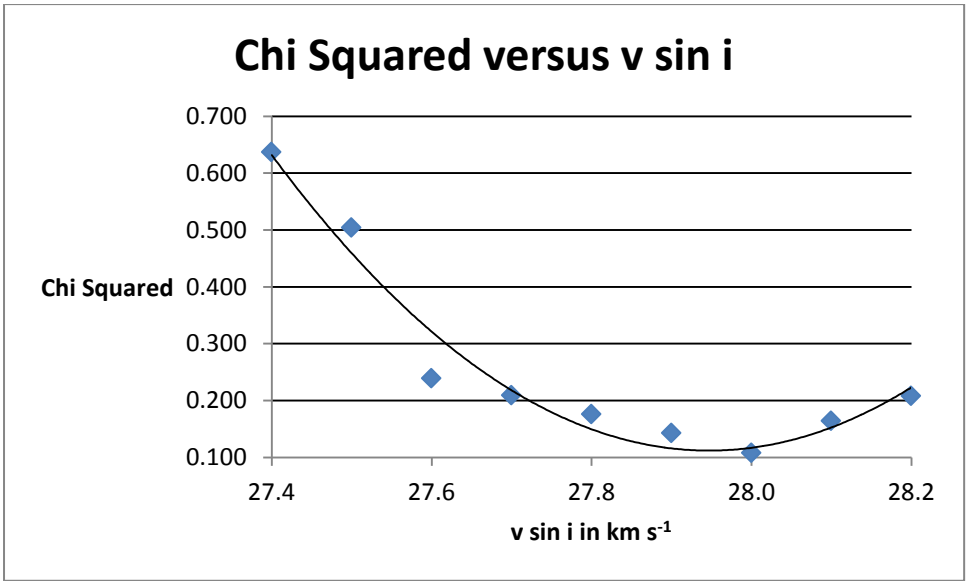

Figure 3.5 Graph of χ2 versus *v* sin *i* for AH Lep.

From the graph *v* sin *i* is selected as 28.0 km s^{-1}. Analysis gives one standard deviation as 0.6 km s^{-1}.

Radius R of a G3V star is 0.98 times that of the Sun.

$$v = \frac{2\pi R}{P} \qquad (9)$$

where *v* is the speed of rotation, R and P the radius and period of the star respectively. Now, *v* sin *i* is 28.0 km s^{-1} where *i* is the inclination angle of the rotational axis with respect to the line of sight. Thus,

$$i = \arcsin \frac{P\, v \sin i}{2\pi R}. \qquad (10)$$

For P = 1.31 days and the radius of the Sun = 6.955 x 10^5 km

$$i = \arcsin \frac{1.31\,\mathrm{d} \times 86\,400\,\mathrm{s\,d^{-1}} \times 28.0 \pm 0.6\,\mathrm{km\,s^{-1}}}{2\pi \times 0.98 \times 6.955 \times 10^5\ \mathrm{km}} = 48 \pm 1°.$$

Nightly Fits to the Data

At each phase of the star's rotation a sequence of four observed intensity profiles (corresponding to the P1-P2-P2-P1 polarisation profiles) can be individually fitted by the model used to generate the starspot mapping. However, as the resulting map for one or two phases is severely unconstrained the map produced is derived from a spaced set of phases.

08 December 2003

On the first night of observation two sets of polarised images in the arrangement P1-P2-P2-P1 were collected. However, more extensive cloud was present during the first cycle and these data have not been included. An optimal extraction method and least squares deconvolution (LSD) technique were applied to each frame. Figure 3.6 shows the maximum entropy fits to the observed LSD profile.

09 December 2003

On the second night of observation two sets of data were obtained with nearly a four hour space between each set. The details of the technique are for the first night. Figure 3.7 shows the maximum entropy fits to the observed LSD profile.

10 December 2003

On the third night of observation one set of data was obtained. The details of the technique and the usefulness of the data are for the first night. Figure 3.8 shows the maximum entropy fits to the observed LSD profile.

11 December 2003

On the fourth night of observation one set of data was obtained. The details of the technique and the usefulness of the data are for the first night. Figure 3.9 shows the maximum entropy fits to the observed LSD profile.

10 December 2008

On the fifth night of observation five years later one set of data was obtained. As no further data were gathered in this epoch no relevant maps are produced.

11 December 2008

As a result of the cloudy conditions no data were obtained on this night.

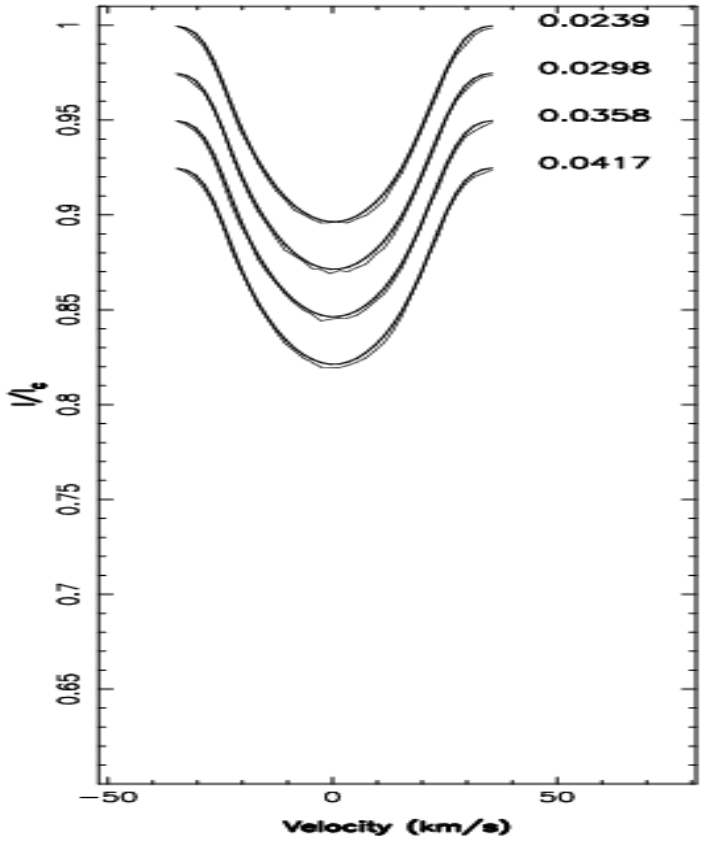

Figure 3.6 Maximum entropy fits to the LSD Stokes I profiles of AH Lep for 08 December 2003. There are thin lines representing the observed profiles and thick lines are the fits produced by the Doppler Imaging code. Each successive image is shifted for graphical purposes. The number to the right of each profile is the rotational phase of the observation.

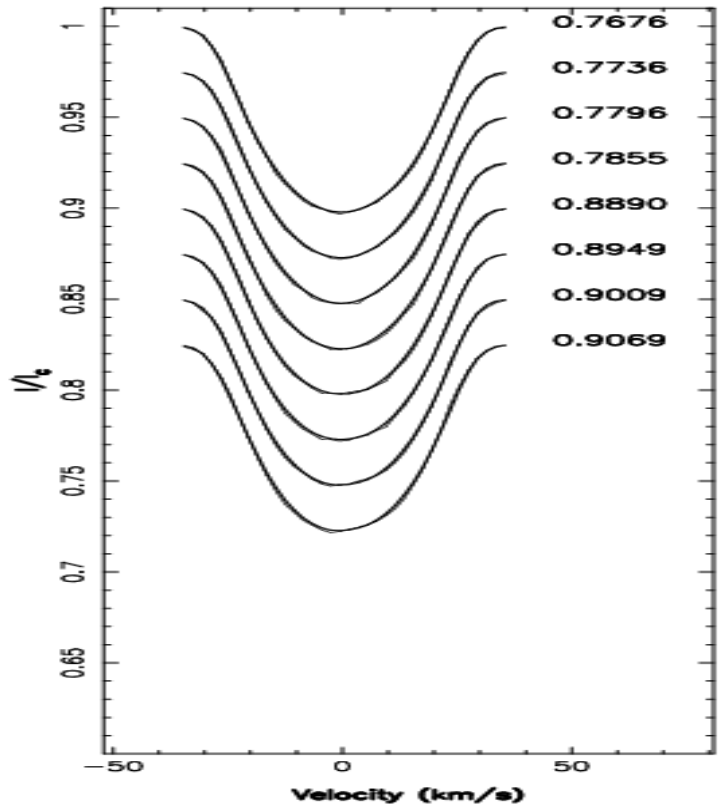

Figure 3.7 Maximum entropy fits to the LSD Stokes I profiles of AH Lep for 09 December 2003. There are thin lines representing the observed profiles and thick lines are the fits produced by the Doppler Imaging code. Each successive image is shifted for graphical purposes. The number to the right of each profile is the rotational phase of the observation.

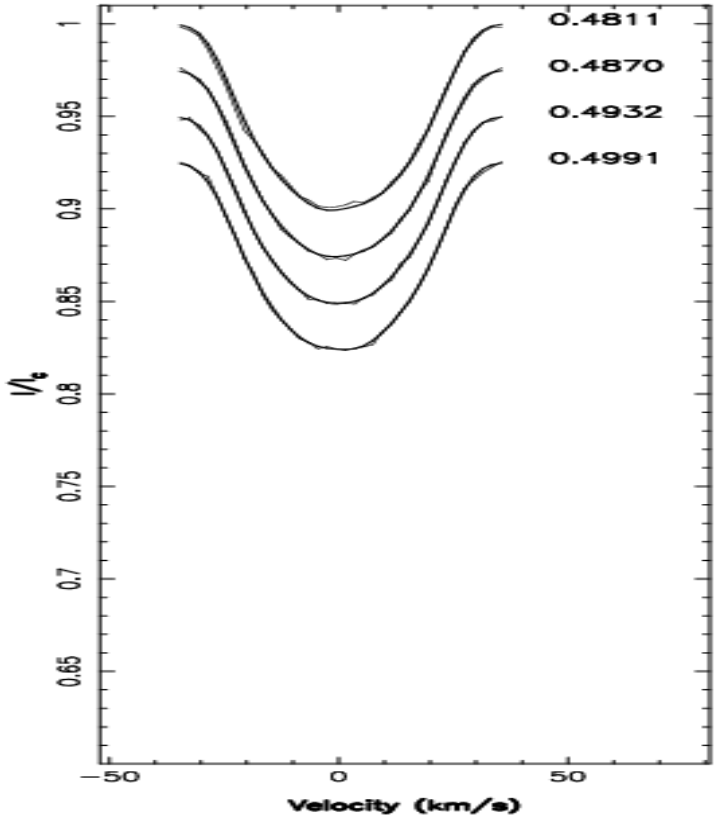

Figure 3.8 Maximum entropy fits to the LSD Stokes I profiles of AH Lep for 10 December 2003. There are thin lines representing the observed profiles and thick lines are the fits produced by the Doppler Imaging code. Each successive image is shifted for graphical purposes. The number to the right of each profile is the rotational phase of the observation.

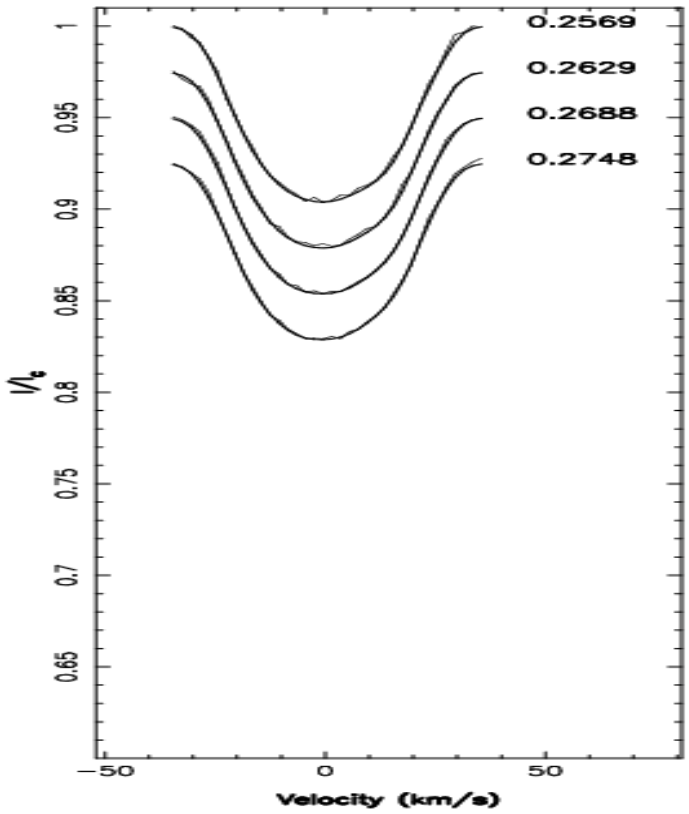

Figure 3.9 Maximum entropy fits to the LSD Stokes I profiles of AH Lep for 11 December 2003. There are thin lines representing the observed profiles and thick lines are the fits produced by the Doppler Imaging code. Each successive image is shifted for graphical purposes. The number to the right of each profile is the rotational phase of the observation.

AH Lep Spot Occupancy Map

For the four nights of observation in December 2003 six sets of data were recorded but five used to construct a brightness map as one set was heavily affected by the combined result of cloud. The 20 images were processed and the Doppler Imaging code applied. Table 3.4 presents the data collected. The total exposure time is the cumulative time over the cycle of four exposures. The signal-to-noise ratios (S/N) are the peak values per pixel for the Stokes I and Stokes V measurements. The S/N_{LSD} ratios are for the relevant deconvolved spectra. The multiplex gain represents the S/N_{LSD} value divided by that for S/N. Figure 3.10 shows the maximum entropy fits to the observed LSD profile and Figure 3.11 displays the brightness map obtained in a polar projection and Figure 3.12 a spherical projection.

Table 3.4 Observations from December 2003 and December 2008 give the Universal Time (UT) start, the stellar exposures from the logs as given in Tables 2.2-2.6, the signal-to-noise ratios for AH Lep for Stokes I and Stokes V measurements and the deconvolved spectra. The multiplex gain is a ratio of the S/N_{LSD} to S/N.

Date and Polarisation Cycle if more than one	UT Start	Stellar Exposures	Total Exposure Time in s	S/N I	S/N V	S/N_{LSD} I	S/N_{LSD} V	Multiplex Gain I	Multiplex Gain V
08/12/03 1	11:11:02.1	31,32, 33,34	2 400	51	36	1 139	2 020	22	56
08/12/03 2	12:07:21.5	35,36, 37,38	2 400	100	92	1291	5 707	13	62
09/12/03 1	11:18:57.2	30,31, 32,33	2 400	120	110	861	4 815	7	44
09/12/03 2	15:07:51.3	55,56, 57,58	2 400	110	100	853	4 295	8	43
10/12/03	09:45:03.3	20,21, 22,23	2 400	63	56	774	2 113	12	38
11/12/03	10:08:30.8	19,20, 21,22	2 400	56	50	777	1 902	14	38
10/12/08	14:55:03	51,52, 53,54	3 600	190	190	844	7 447	4	39

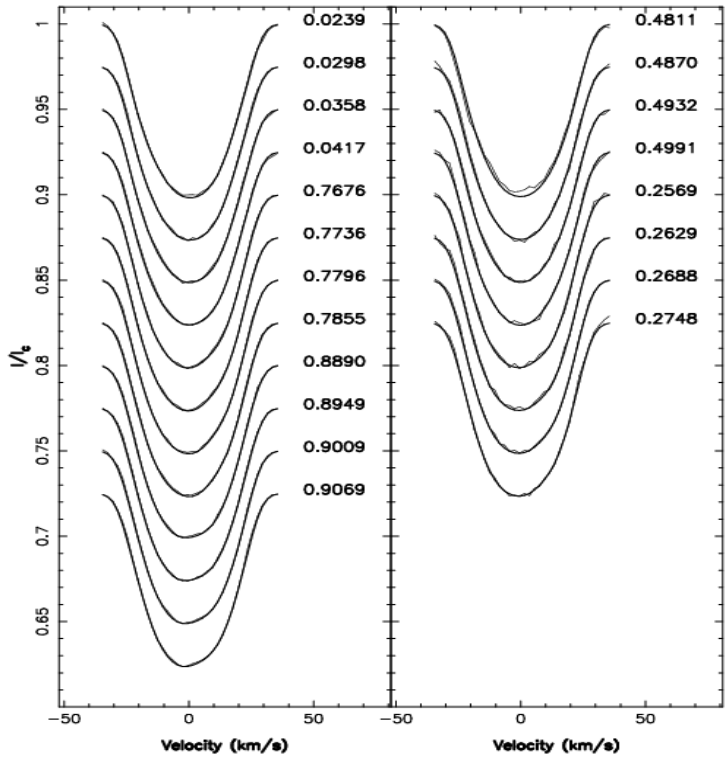

Figure 3.10 Maximum entropy fits to the LSD Stokes I profiles of AH Lep for 20 exposures on 08, 09, 10 and 11 December 2003. There are thin lines representing the observed profiles and thick lines are the fits produced by the Doppler Imaging code. Each successive image is shifted for graphical purposes. The number to the right of each profile is the rotational phase of the observation.

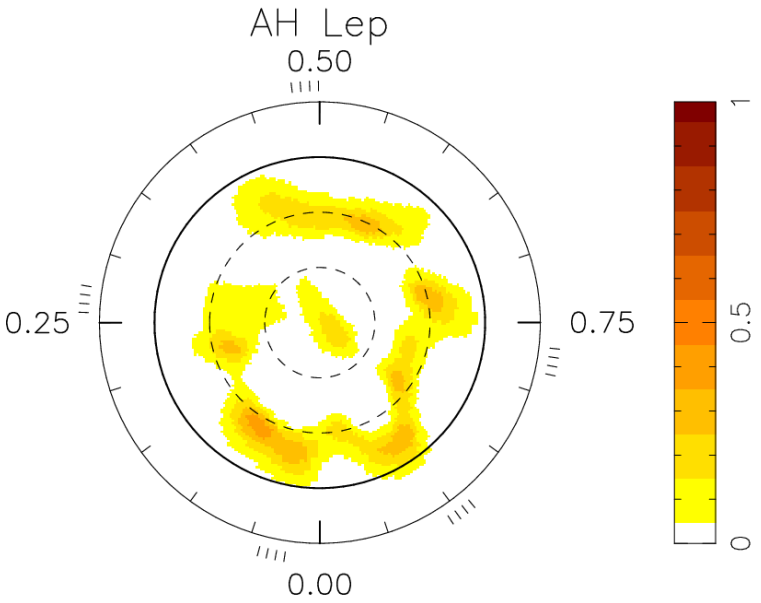

Figure 3.11 Maximum entropy brightness image combined for 08, 09, 10 and 11 December 2003. The image is a flattened polar projection. The radial ticks outside the plot give the phases of observation. The dotted circles from the centre are latitudes of +60° and +30°, the complete circle is the equator and the outside circle extends to -30°. The coloured bar indicates a gradation of spottedness with 0 (absent) to 1 (most intense).

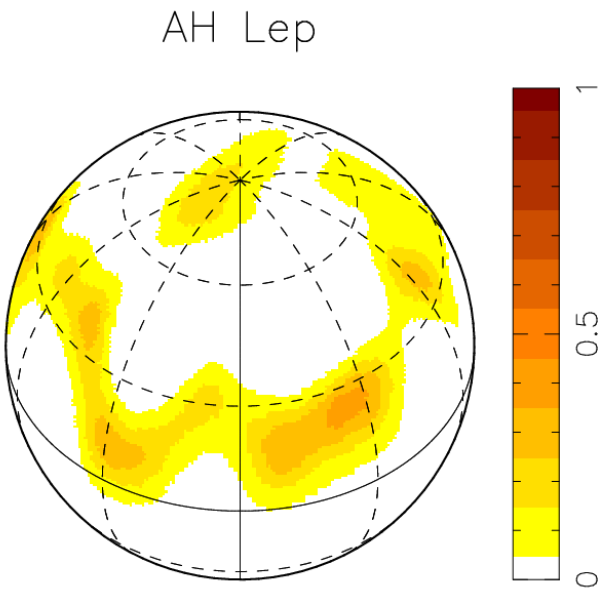

Figure 3.12 Maximum entropy brightness image combined for 08, 09, 10 and 11 December 2003. The image is a spherical projection. The circles from the top are +60°, +30°, equator and -30°. The coloured bar indicates a gradation of spottedness with 0 (absent) to 1 (most intense).

The combined image does not have a prominent polar spot which is typical of a number of other young solar proxy stars but there are a number of weak mid-latitude features. The total spot coverage is 3.3% of the entire stellar disc.

As a contrast Figure 3.13 is a display of R58 by Marsden et al. 2005. There is a significant polar spot and the total spot coverage is 13%.

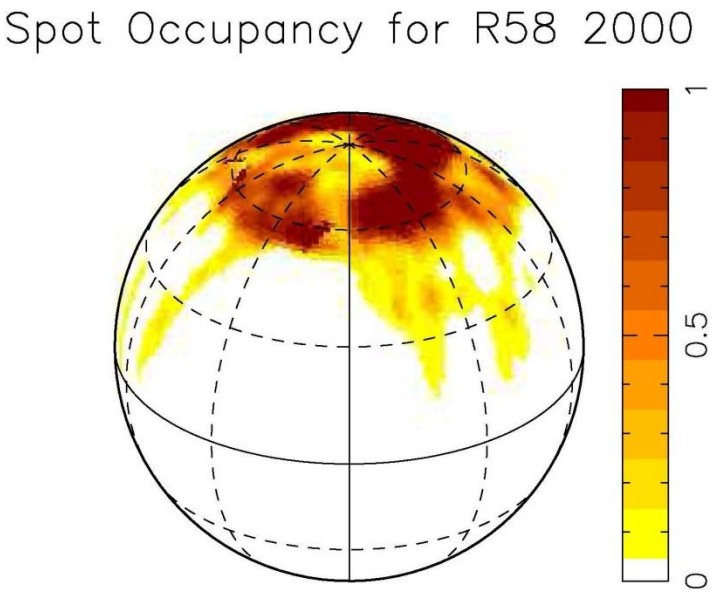

Figure 3.13 Maximum entropy brightness image for R58 from Marsden et al. 2005. The image is a spherical projection. The circles from the top are +60°, +30°, equator and -30°. The large polar spot contributes significantly to the 13% total spot coverage.

3.4 Results of Zeeman Doppler Imaging of AH Lep for 2003

Zeeman Doppler Imaging allows the construction of a map showing the magnetic tomography of AH Lep. In addition to a display of the position of the magnetic regions the plot reveals the orientation of the magnetic features.

ZDI observations of AH Lep (HD 36869) on 08, 09, 10 and 11 December 2003 were made with the instrumentation described in Chapter 2. Five usable cycles of polarisation were conducted. The resulting Stokes *V* profiles (including the first set which was not used due to cloud) are shown in Figure 3.14.

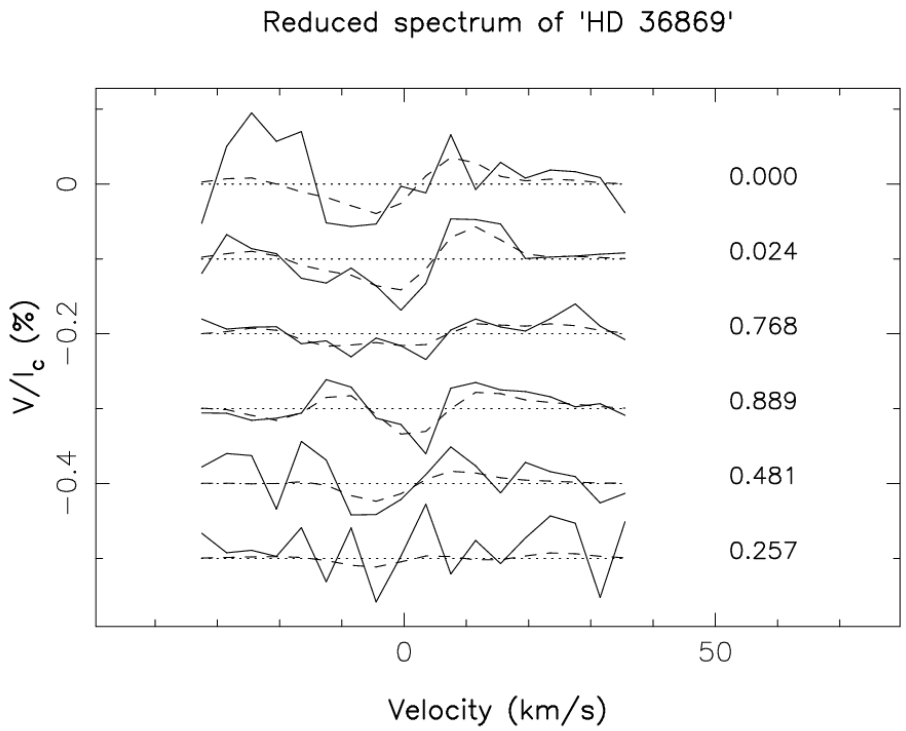

Figure 3.14 Maximum entropy fits (continuous line) to the LSD Stokes *V* profiles (dashed line) of AH Lep (HD 36869) for 08, 09, 10 and 11 December 2003. The dotted line in each is the zero circular polarisation level of each profile. Each successive image is shifted for graphical purposes. The number to the right of each profile is the rotational phase of the observation.

Reconstructed spherical projection maps are displayed in Figure 3.15. The first displays the brightness map of Figure 3.12. Then each component of the magnetic field is generated. The radial magnetic field is perpendicular to the stellar surface. The azimuthal element is also known as the toroidal component and the meridional display as the poloidal element.

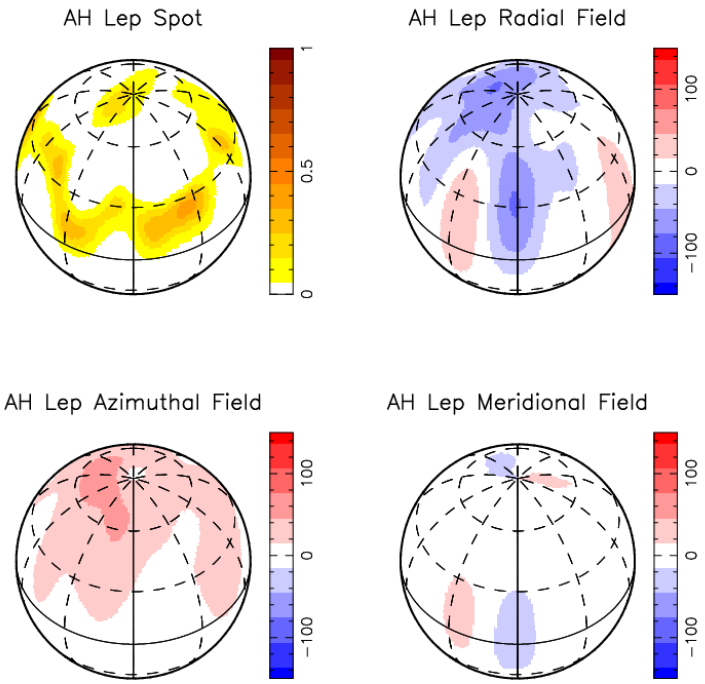

Figure 3.15 Spherical projection of maximum entropy reconstructed magnetic maps of AH Lep for combined observations on 08, 09, 10 and 11 December 2003. The spot map gives the brightness, radial field is at right angles to surface, azimuthal (toroidal) is in the direction of lines of latitude and meridional (poloidal) is between the poles. The scale on the three magnetic maps is in gauss.

3.5 Discussion

AH Lep is a G3V star with a period of 1.31 day and age less than 50 x 10^6 years. It has a spot occupancy of 3.3%.

The brightness and magnetic maps of Figure 3.15 do not display a significant polar spot. The idea that polar spotting is a necessary element of young, solar-type rapid rotators is no longer held. Indeed, Strassmeier (2002) examined 65 stars mapped with the Doppler Imaging technique and found that 36 (55%) showed a prominent polar spot, some up to 20% occupancy but that leaves a sizable proportion without such intense spotting.

Five other young early G stars have been researched for their spot topology. Four have a reasonable polar spot: R58 has a B-V value of 0.61 (Marsden et al. 2005), LQ

Lup with a B-V value of 0.69 (Donati et al. 2000), HD 171488 of 0.62 B-V (Marsden et al. 2006) and HD 106506 having a B-V value of 0.60 (Waite et al. 2010 submitted). However, the polar spot on HD 141943 with a B-V of 0.65 (Marsden et al. 2010 in preparation) is significantly smaller than the four preceding examples. The polar spot on AH Lep with a B-V value of 0.64 is more akin to that of HD 141943.

The data allow the construction of a graph of fractional spottedness versus latitude defined by

$$F(\ell) = \frac{S(l)\cos(l)\,dl}{2} \qquad (11)$$

where F(ℓ) is the fractional spottedness at latitude ℓ and S(ℓ) is the average spot occupancy at latitude ℓ. This is displayed in Figure 3.16.

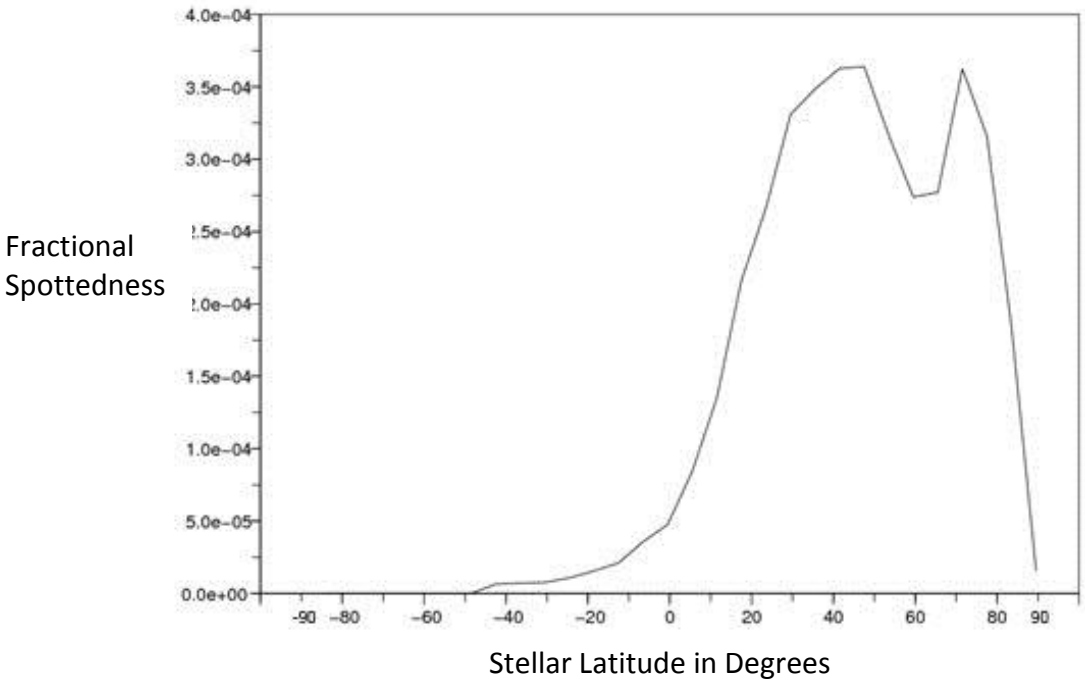

Figure 3.16 Fractional spottedness versus stellar latitude for AH Lep based on the average spot occupancy at each latitude as defined by equation 11.

The brightness maps of Figures 3.11 and 3.12, the top left hand map of Figure 3.15 and the fractional spottedness graph of Figure 3.16 show very little in the way of a polar spot with features present in the latitudes of +20° and +80° but predominantly

between +30° to + 75°. There is a ring of spottedness in the azimuthal (toroidal) direction around the pole for AH Lep. HD 171488 (Marsden et al. 2006) and HD 106506 (Waite et al. 2010 submitted) also display such a feature. It is this which has fuelled the belief that the mechanism within the star is one of a distributed dynamo. Solanki (2002) suggests that this effect is due to differential rotation. Unfortunately, insufficient data have been collected on AH Lep over a number of cycles to produce differential rotation measurements.

The magnetic flux in gauss may be plotted against stellar latitude for the components of the magnetic field. Figure 3.17 shows the radial element where positive indicates the field lines perpendicular to the stellar surface and directed outwards and negative inwards.

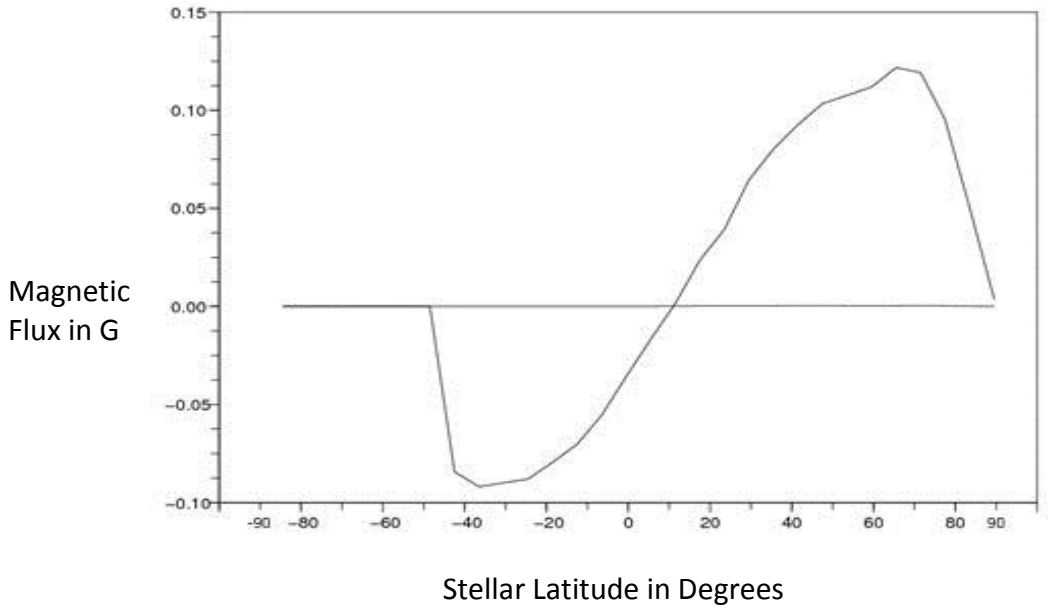

Figure 3.17 Magnetic flux in gauss for the radial component versus stellar latitude for AH Lep. Positive is the direction of the field perpendicular to the surface outwards and negative inwards.

The top right map of Figure 3.15 shows a positive radial field straddling the equator and a negative field around the pole and some parts extending beyond the

equator. Figure 3.17 displays a peak of positive field of 1.3 x 10^{-1} G around +65° and negative of absolute value 8 x 10^{-2} G at -40°.

The toroidal (azimuthal) magnetic field is in the direction of the lines of latitude and positive defined as counterclockwise around the rotational axis of the star. This component is mapped in Figure 3.18.

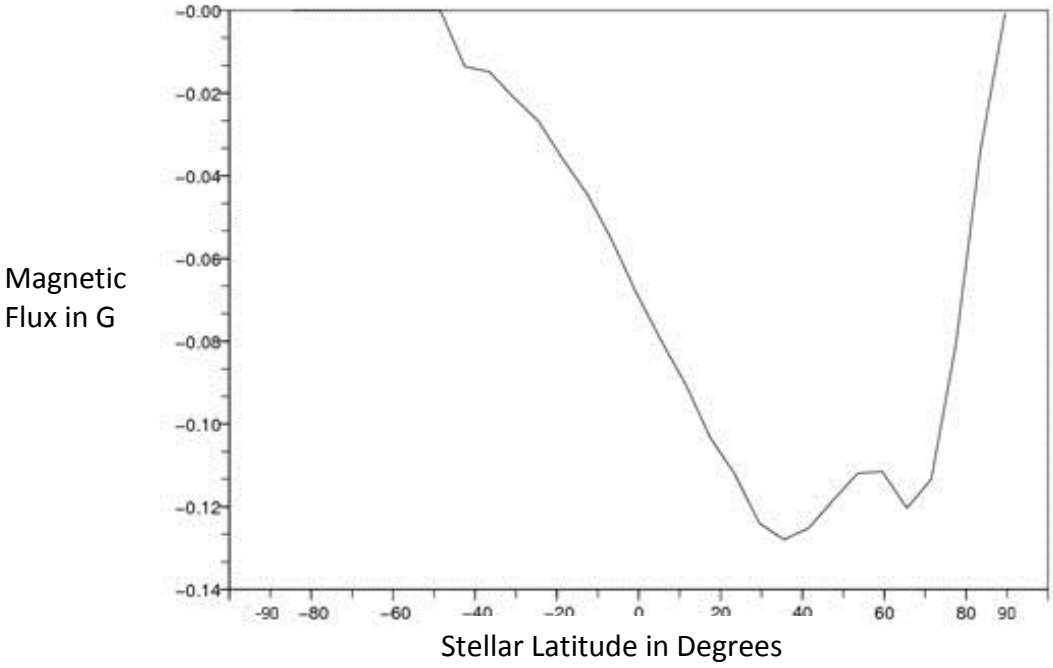

Figure 3.18 Magnetic flux in gauss for the toroidal (azimuthal) component versus stellar latitude for AH Lep. Positive is counterclockwise around the rotational axis of the star.

The toroidal component is clockwise around the rotational axis of AH Lep and peaks around +40° with an absolute value of 1.3 x 10^{-1} G.

The poloidal (meridional) magnetic field is parallel with the star's rotational axis with positive being towards the pole inclined towards the line of sight. This map is displayed in Figure 3.19.

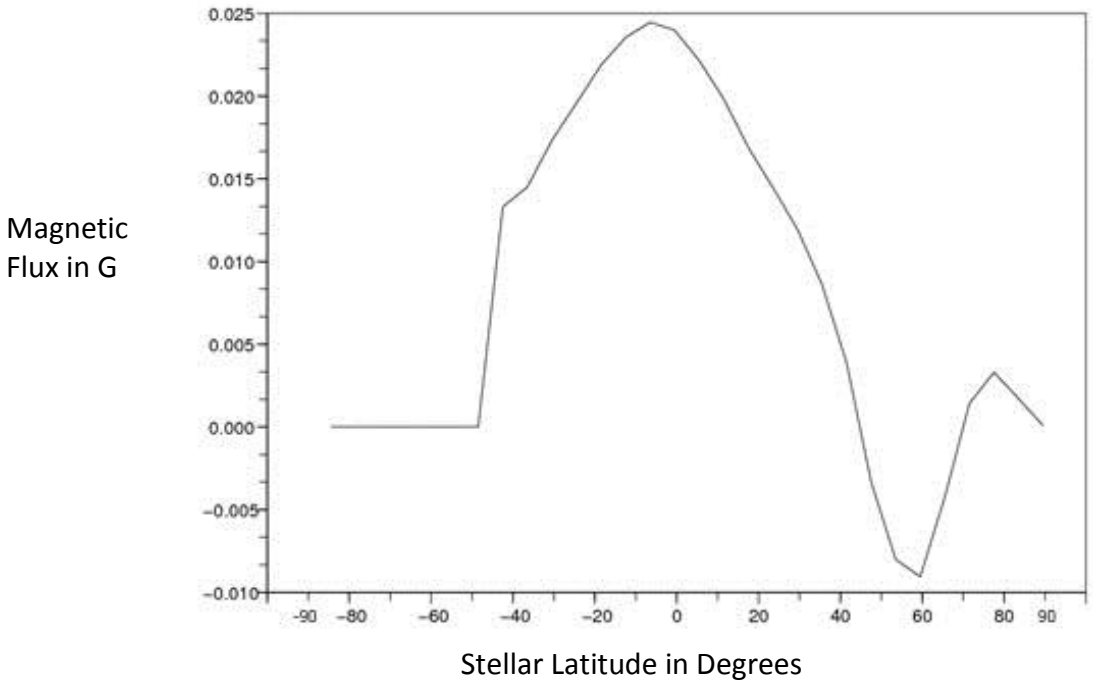

Figure 3.19 Magnetic flux in gauss for the poloidal (meridional) component versus stellar latitude for AH Lep. Positive is in the poleward direction.

Results from Figure 3.19 suggest a 2.5 x 10^{-2} G peak of poloidal magnetic flux just below the equator of AH Lep towards the pole. The poloidal component of the magnetic field on AH Lep is very small compared with the toroidal contribution. This fits with the summary of Petit et al. (2008) where the magnetic field is mostly poloidal for low rotation rates but more rapid rotators host a large-scale toroidal component in their surface field. Their cut-off figure was 12 days: any lower rotational period permitted the toroidal magnetic energy to dominate the poloidal component. Also, the amount of the toroidal component tends not to support the presence of a solar-type dynamo. It is not inconsistent with the concept of a distributed dynamo. Brown et al. (2009 submission) have produced models to show that young solar-type stars with periods of 5-9 days are

able to produce a magnetic field and sustain it without the existence of an interface layer.

It is suggested that solar-type stars probably had more extensive magnetic fields earlier in their existence. Magnetic stellar winds cause the loss of angular momentum (Güdel et al. 1997) and the rate of loss due to this braking effect depends basically on angular velocity and spectral type (Messina et al. 2003).

It is important to image a star over an entire cycle and over a significant amount of time. Berdyugina (2005) pursued II Peg over six months and discovered that as one active longitude reduces another increases so that there was a redistribution of spotted areas between the opposite hemispheres. Also, Marsden et al. (2010 in preparation) found the poloidal versus toroidal fraction on HD 141943 was 47% in 2007 but 82% in 2009.

AH Lep has shown that it is worthy of further research. A magnetic field has been detected. However, a complete coverage of a cycle has not been observed. Also, just as the Sun undergoes a 22 year cycle of activity, AH Lep ought to be followed for a number of years to build up a more complete picture of its activity.

3.6 Conclusion

The starspot features and magnetic field of AH Lep have been investigated with the techniques of Doppler and Zeeman Doppler Imaging. This G3V star is a suitable proxy for the young Sun. At the time of observation there was little in the way of a polar spot but this rapid rotator has a reasonable toroidal magnetic component. It is a good candidate for a longitudinal study to join other stars that can assist in building a picture of the early evolution of our Sun.

The results presented in this thesis support AH Lep's hypothesised appearance, with starspot features intermediate between those of between very rapidly rotating solar-type stars and the Sun today. The magnetic results presented here are less conclusive but are consistent with a distributed dynamo acting in this young solar proxy that contrasts with the interface-layer dynamo acting in the Sun today.

Further ZDI observations of AH Lep are clearly warranted to confirm the tentative results outlined in this thesis. Such studies should include high signal-to-noise data for improved magnetic maps, observing runs spanning a week or so at a time to attempt differential rotation measurements and repeated observations at yearly intervals to monitor any changes that provide the empirical basis for a stellar magnetic cycle or other changes in spot features or the underlying dynamo. Improved observations of AH Lep using ZDI at the AAT can then more confidently use this star to test stellar dynamo theory and provide a proxy for studies of early solar evolution.

References

Babcock, H W (1961). The topology of the Sun's magnetic field and the 22-year cycle. The Astrophysical Journal, 133, 572.

Bahcall, J N, Pinsonneault, M H, Basu, S (2001). Solar Models: Current Epoch and Time Dependencies, Neutrinos and Helioseismological Properties. The Astrophysical Journal, 555, 990.

Barnes, S A (2003). On the Rotational Evolution of Solar- and Late-type Stars, Its Magnetic Origins, and the Possibility of Stellar Gyrochronology. The Astrophysical Journal, 586, 464.

Berdyugina, S V (2005). Starspots: A Key to the Stellar Dynamo. Living Reviews in Solar Physics, 2, 8.

Bernasconi, P A, Maeder, A (1996). About the absence of a proper zero age main sequence for massive stars. Astronomy and Astrophysics, 307, 829.

Brown, S F., Donati, J.-F, Rees, D E, Semel, M (1991). Zeeman-Doppler Imaging of solar-type and Ap stars. Astronomy and Astrophysics, 250, 463.

Brown, B P, Browning M K, Brun, A S, Miesch M S, Toorme, J (2009 submission). The Astrophysical Journal.

Burleigh, M R, Barstow, M A, Holberg, J B (1998). A search for hidden white dwarfs in the ROSAT EUV survey – II., Discovery of a distant DA+F6/7V binary system in a direction of low-density neutral hydrogen. Monthly Notices of the Royal Astronomical Society, 300, 511.

Carroll, B W, Ostlie, D A (2007). An Introduction to Modern Astrophysics. second edition, San Francisco: Addison Wesley.

Carter, B, Brown, S, Donati, J.-F, Rees, D, Semel, M (1996). Zeeman Doppler Imaging of Stars with the AAT. Astronomical Society of Australia, 13, 150.

Collier Cameron, A (1992). Modeling stellar photospheric spots using spectroscopy in Byrne, P B and Mullan, D J (eds). Surface inhomogeneities on late-type stars. Lecture Notes in Physics, volume 397 Heidelberg, Germany: Springer-Verlag.

Collier Cameron, A, Jianke, L (1994). Magnetic braking of G and K dwarfs without core-envelope decoupling. Monthly Notices of the Royal Astronomical Society, 269, 1099.

Collier Cameron, A, (2000) Mapping Starspots and Magnetic Fields on Cool Stars, talk given to International Astronomical Union Symposium 203, Manchester, United Kingdom.

Collier Cameron, A, Donati, J-F (2002). Doin' the twist: secular changes in the surface differential rotation on AB Doradus. Monthly Notices of the Royal Astronomical Society, 329, 23.

Collier Cameron, A, Donati, J-F, Semel, M (2002). Stellar differential rotation from direct star-spot tracking. Monthly Notices of the Royal Astronomical Society, 330, 699.

Cutispoto, G, Pastori, L, Tagliaferri, G, Messina, S, Pallavicini, R (1999). Classification of EUV stellar sources detected by the ROSAT WFC. Astronomy and Astrophysics Supplement Series, 138, 87.

Cutispoto, G, Pastori, L, Pasquini, L, de Medeiros, J R, Tagliaferri, G, Andersen, J (2003a). Fast-rotating Nearby Solar-type Stars. Proceedings of 12th Cambridge Workshop on Cool Stars, Stellar Systems and The Sun, University of Colorado.

Cutispoto, G, Tagliaferri, G, de Medeiros, J R, Pastori, L, Pasquini, L, Andersen, J (2003b). Fast-rotating nearby solar-type stars II. Li abundances, *v* sin *i* and X-ray luminosities relationships. Astronomy and Astrophysics, 397, 987.

Donati, J-F, Semel, M, Praderie, F (1989). Zeeman-Doppler imaging of active stars II. Numerical simulation and first observational results. Astronomy and Astrophysics, 225, 467.

Donati, J-F, Brown, S F, Semel, M, Rees, D E, Dempsey, R C, Matthews, J M, Henry, GW, Hall, D S. (1992). Photospheric imaging of the RS CVn system HR 1099. Astronomy and Astrophysics, 265, 682.

Donati, J-F, Semel, M, Carter, B D, Rees, D E, Collier Cameron, A (1997). Spectropolarimetric observations of active stars. Monthly Notices of the Royal Astronomical Society, 291, 658.

Donati, J-F, Brown, S F (1997). Zeeman-Doppler imaging of active stars V. Sensitivity of maximum entropy magnetic maps to field orientation. Astronomy and Astrophysics, 326, 1135.

Donati, J-F, Collier Cameron, A (1997). Differential rotation and magnetic polarity patterns on AB Doradus. Monthly Notices of the Royal Astronomical Society, 291, 1.

Donati, J-F (1999). Magnetic cycles of HR 1099 and LQ Hydrae. Monthly Notices of the Royal Astronomical Society, 302, 457.

Donati, J-F, Collier Cameron, A, Hussain, G A J, Semel, M (1999). Magnetic topology and prominence patterns on AB Doradus. Monthly Notices of the Royal Astronomical Society, 302, 437.
Donati, J-F, Mengel, M, Carter, B D, Marsden, S, Collier Cameron, A, Wichmann, R (2000). Surface differential rotation and prominences of the Lupus post T Tauri star RX J1508.6-4423. Monthly Notices of the Royal Astronomical Society, 316, 699.

Donati, J-F (2003). ESPaDOnS: An Echelle SpectroPolarimetric Device for the Observation of Stars at CFHT. Astronomical Society of the Pacific Conference Series, eds. Bueno J T, Almeida, J S, 307.

Donati, J-F, Collier Cameron, A, Semel, M, Hussain, G A J, Petit, P, Carter, B, Mengel, M, Marsden, S C, Ariste, A López, Rees, D E (2003a). Dynamo processes and activity cycles of the active stars AB Doradus, LQ Hydrae and HR 1099. Monthly Notices of the Royal Astronomical Society, 345, 1145.

Donati, J-F, Collier Cameron, A, Petit, P (2003b). Temporal fluctuations in the differential rotation of cool active stars. Monthly Notices of the Royal Astronomical Society, 345, 1187.

Dorren, J D, Guinan, E F (1994). HD 129333: The Sun in its Infancy. The Astrophysical Journal, 428, 805.

Freedman, R A, Kaufmann, W J (2005). Universe. seventh edition, W H Freeman and Company, New York.

Granzer, T, Schüssler, M, Caligari, P, Strassmeier, K G (2000). Distribution of starspots on cool stars. II. Pre-main-sequence and ZAMS stars between 0.4 M and 1.7 M. Astronomy and Astrophysics, 355, 1087.

Güdel, M, Guinan, E F, Skinner, S l (1997). The X-Ray Sun in Time – A Study of the Long-Term Evolution of Coronae of Solar-Type Stars. The Astrophysical Journal, 483, 747.

Guinan, E F, Engle, S G (2009). The Sun in Time: Age, Rotation, and Magnetic Activity of the Sun and Solar-type stars and Effects on Hosted Planets. The Ages of Stars Proceedings IAU Symposium No. 258, E E Mamajek and D Soderblom eds.

Hussain, G A J (1999). Magnetic activity in late-type stars. Ph.D. submission, The University of St Andrews.

Kitchin, C R (2003). Astrophysical Techniques. fourth edition, Institute of Physics Publishing, Bristol.

Lister, T, Metcalfe, T, Brown, T, Street, R (2009). Temporal Variability of Stars and Stellar Systems. A White Paper for the Stars and Stellar Evolution Science Frontier Panel of the Astro2010 Decadal Survey.

Macquarie Dictionary (2002), revised third edition, The Macquarie Library Pty Ltd, Macquarie University.

Marsden, S C, Waite, I A, Carter, B D, Donati, J-F (2004). Doppler imaging of G-dwarfs in two young open clusters. Astronomische Nachrichten, 325, 246.

Marsden, S C, Waite, I A, Carter, B D, Donati, J-F (2005). Doppler imaging and surface differential rotation of young open cluster stars I. HD 307938 (R58) in IC 2602. Monthly Notices of the Royal Astronomical Society, 359, 711.

Marsden, S C, Donati, J-F, Semel, M, Petit, P, Carter, B D (2006). Surface differential rotation and photospheric magnetic field of the young solar-type star HD 171488 (V889 Her). Monthly Notices of the Royal Astronomical Society, 359, 791.

Marsden, S C, Jardine, M M, Ramirez, J C, Brown, C A, Carter, B D, Donati, J-F, Dunstone, N, Hart, R, Semel, M, , Waite, I A, (2010 in preparation). Magnetic fields and differential rotation on the pre-main sequence I : The early-G star HD 141943.

Mengel, M W (2006). The Active Young Solar-Type Star HR 1817 (-HD 35850). Master of Philosophy thesis, University of Southern Queensland, Toowoomba.

Messina, S, Rodonò, M, Guinan, E F (2001). The "rotation-activity connection": Its extension to photospheric activity diagnostics. Astronomy and Astrophysics, 366, 215.

Messina, S, Pizzolato, N, Guinan, E F, Rodonò, M (2003). Dependence of coronal X-ray emission on spot-induced brightness variations in cool main sequence stars. Astronomy and Astrophysics, 410, 671.

Montes, D, Laópez, J, Gálvez, M C, Fernández-Figueroa, M J, De Castro, E, Cornide, M (2001). Late-type members of young stellar kinematics groups – I. Single stars. Monthly Notices of the Royal Astronomical Society, 328, 45.

Petit, P, Donati, J-F, Collier Cameron, A (2002). Differential rotation of cool active stars: The case of intermediate rotators. Monthly Notices of the Royal Astronomical Society, 334, 374.

Petit, P, Dintrans, B, Solanski, S K, Donati, J-F, Aurière, M, Lignières, F, Morin, J, Paletou, F, Ramirez, J, Catala, C, Fares, R (2008). Toroidal vs poloidal magnetic fields in Sun-like stars: a rotation threshold. Monthly Notices of the Royal Astronomical Society, 388, 80.

Rice, J B, Wehlau, W H, Khokhlova, V L (1989). Mapping stellar surfaces by Doppler imaging – Technique and application. Astronomy and Astrophysics, 208, 179.

Samus, N N, Durlevich, O V et al. (2004 edition). Combined General Catalog of Variable Stars, GCVS42.

Schrijver, C J, Zwaan, C (2000). Solar and stellar magnetic activity. Cambridge Astrophysics Series, Cambridge: Cambridge University Press.

Schüssler, M, Solanki, S K (1992), Why rapid rotators have polar spots. Astronomy and Astrophysics, 264, L13.

Schüssler, M, Caligari, P, Ferriz-Mas, A, Moreno-Insertis, F 1994. Variable Solar and Stellar Activity by a Flux Tube Dynamo. Astronomy and Astrophysics, 281, L69.

Schüssler, M, Caligari, P, Ferriz-Mas, A, Solanki, S K, Stix, M (1996). Distribution of starspots on cool stars. I. Young and main sequence stars of 1 M. Astronomy and Astrophysics, 314, 503.

Semel, M (1989). Zeeman-Doppler imaging of active stars I. Basic principles. Astronomy and Astrophysics, 225, 456.

Semel, M, Donati, J-F, Rees, D E (1993). Zeeman-Doppler imaging of active stars III. Instrumental and technical considerations. Astronomy and Astrophysics, 278, 231.

Solanki, S.K. 2002. The magnetic structure of sunspots and starspots. Astronomische Nachrichten, 323 165.

Strassmeier, K G, Rice, J B (1998). Doppler imaging of stellar surface structure. VI. HD 129333 = EK Draconis: A stellar analog of the active young Sun. Astronomy and Astrophysics, 330, 685.

Strassmeier, K G (2001). Latest results in Doppler imaging. Page 271 of: Garcia, R J, Lopez, R R, Osorio, M RZ (eds) Cool stars, stellar systems, and the Sun. 11th Cambridge workshop, Astronomical Society of the Pacific Conference Proceedings, vol 223. San Francisco: Astronomical Society of the Pacific.

Strassmeier, K G (2002). Doppler images of starspots. Astronomische Nachrichten. 323, 309.

Vogt, S S, Penrod, G D (1983). Doppler imaging of spotted stars – Application to the RS Canum Venaticorum star HR 1099. Publications of the Astronomical Society of the Pacific, 95, 565.

Vogt, S S, Penrod, G D, Hatzes, A P (1987). Doppler images of rotating stars using maximum entropy image reconstruction. The Astrophysics Journal, 321, 496.

Waite, I A, Marsden, S C, Ramírez J, Dunstone, N, Hart, R, Carter, B D (2010 submitted). Differential Rotation and Surface Magnetic Fields of the Active Young Star HD 106506.

Weber, M, Strassmeier, K G, Washuettl, A (2005). Indications for anti-solar differential rotation of giant stars. Astronomische Nachrichten, 326, 287.

Wetherill, G W (1980). Formation of the Terrestrial Planets. Annual Review of Astronomy and Astrophysics, 18, 117.

Wichmann, R, Schmitt, J H M M (2003). Field zero-age main-sequence stars in the solar neighbourhood: where have they come from? Monthly Notices of the Royal Astronomical Society, 342, 1021.

Wichmann, R, Schmitt, J H M M, Hubrig, S (2003). Nearby young stars. Astronomy and Astrophysics, 399, 983.

Zuckerman, B, Song, I, Bessell, M S, Webb, R A (2001). The β Pictoris Moving Group. The Astrophysical Journal, 562, L87.

http://cct.rncan.gc.ca/glossary/index_e.php?id=3173

http://media.skyandtelescope.com/images/Sunspot-group_l.jpg

http://sohowww.nascom.nasa.gov/gallery/Helioseismology/mdi013.html

http://star-www.st-and.ac.uk/~acc4/coolpages/cartoon.gif

http://www.aao.gov.au

http://www.astro.ljmu.ac.uk/courses/phys362/notes/img94.png

http://www.ifa.hawaii.edu/~barnes/ast110_06/tsaas/1003a.jpg

http://upload.wikimedia.org/wikipedia/commons/9/93/Sunspot_butterfly_with_graph.jpg

mstecker.com/pages/australiaphotos1_fp.htm